

# Supporting Information

for

## **Naphthalimide–phenothiazine dyads: effect of conformational flexibility and matching of the energy of the charge-transfer state and the localized triplet excited state on the thermally activated delayed fluorescence**

Kaiyue Ye<sup>\*1</sup>, Liyuan Cao<sup>\*1</sup>, Davita M. E. van Raamsdonk<sup>\*2</sup>, Zhijia Wang<sup>1</sup>, Jianzhang Zhao<sup>\*1,3</sup>, Daniel Escudero<sup>\*2</sup>, and Denis Jacquemin<sup>\*4</sup>

Experimental procedures, characterization data, <sup>1</sup>H and <sup>13</sup>C NMR spectra of compounds, mass spectra and Spectral data

## Table of contents

1. General information.....	S2
2. Synthesis of the compounds.....	S2
3. Molecular structure characterization data.....	S5
4. Steady state UV–vis absorption and luminescence spectra.....	S20
5. Fluorescence lifetimes.....	S22
6. Phosphorescence spectra.....	S22
7. Phosphorescence lifetimes.....	S23
8. Spectroelectrochemistry measurement.....	S24
9. Nanosecond transient absorption spectroscopy.....	S25
10. Calculated study.....	S30

# 1. General Information

All the chemicals used in synthesis are analytically pure and were used as received. Solvents were dried and distilled prior to use.  $^1\text{H}$  and  $^{13}\text{C}$  NMR spectra were recorded on the Bruker Avance spectrometers (400 / 500 / 600 MHz).  $^1\text{H}$  and  $^{13}\text{C}$  chemical shifts are reported in parts per million (ppm) relative to TMS, with the residual solvent peak used as an internal reference. The mass spectra were measured by HRMS (MALDI-TOF), HRMS (EI-TOF) and HRMS (ESI-TOF). UV-vis absorption spectra were measured on a Shimadzu UV-2550 UV-vis spectrophotometer. Fluorescence spectra were recorded with an Edinburgh instruments FS5 spectrofluorometer. Luminescence lifetimes of compounds were recorded with an OB920 luminescence lifetime spectrometer (Edinburgh Instruments, U.K.). All these calculations were performed with Gaussian 09W.<sup>1</sup> Natural transition orbital analysis were performed by the Multiwfn program.<sup>2</sup>

## 2. Synthesis of the compounds

**2.1. Synthesis of 2.** A mixture of **NI-3Br** (3.0 g, 7.750 mmol), bis(pinacolato)diboron (2.0 g, 7.750 mmol), KOAc (1.5 g, 15.5 mmol) and Pd(dppf)Cl<sub>2</sub> (257.4 mg, 0.320 mmol) in toluene (77ml) was degassed by gently bubbling N<sub>2</sub> for 30 min. The mixture stirred at 110 °C for 16 h. After cooling, it was extracted with CH<sub>2</sub>Cl<sub>2</sub> (100 mL × 3). The combined organic layer was washed with water (100 mL), brine solution (100 mL), dried over anhydrous Na<sub>2</sub>SO<sub>4</sub>, filtered and evaporated to dryness. The crude product was purified by column chromatography (silica gel, DCM:PE = 1:6, v/v) to give white solids **2** (400 mg, 11.9%).  $^1\text{H}$  NMR (CDCl<sub>3</sub>, 400 MHz)  $\delta$ : 0.86–0.94 (m, 6H), 1.30–1.37 (m, 8H), 1.40 (s, 12H), 1.92–1.96 (m, 1H), 4.08–4.19 (m, 2H), 7.75 (m,  $J$  = 15.51 Hz, 1H), 8.23 (d,  $J$  = 8.13 Hz, 1H), 8.62 (d,  $J$  = 25.01 Hz, 1H), 8.67 (s, 1H), 8.99 (s, 1H).  $^{13}\text{C}$  NMR (CDCl<sub>3</sub>, 125 MHz)  $\delta$ : 164.63, 164.46, 138.00, 136.49, 134.07, 132.22, 131.73, 130.20, 127.84, 126.86, 123.82, 122.79, 84.56, 44.18, 37.96, 30.80, 28.77, 24.95, 24.13, 23.09, 10.58. HRMS (MALDI,  $m/z$ ) calcd for C<sub>38</sub>H<sub>64</sub>N<sub>2</sub>O<sub>2</sub>S [M+H]<sup>+</sup>, 435.2581, found 436.2665.

**2.2. Synthesis of NI-Ph-Br.** Under N<sub>2</sub> atmosphere, Compound 2 (61.1 mg, 0.141 mmol) and 1-bromo-4-iodobenzene (75.0 mg, 0.265 mmol) were dissolved in mixed solvent of toluene (3 ml), ethanol (0.8 ml) and water (0.5 ml), followed by the addition of K<sub>2</sub>CO<sub>3</sub> (70.0 mg, 0.506 mmol). After bubbling with N<sub>2</sub> for 20 min, Pd(PPh<sub>3</sub>)<sub>4</sub> (30 mg, 0.026 mmol) was added, and the mixture was refluxed for 8 h. Then the reaction was cool to room temperature and extracted by dichloromethane. The organic layer was dried over anhydrous Na<sub>2</sub>SO<sub>4</sub> and concentrated under reduced pressure to attain the crude product. The residue was purified by column chromatography (silica gel, DCM:PE = 1:2, v/v) to afford compound **NI-Ph-Br** as pale white solid (64 mg, 92.9%). <sup>1</sup>H NMR (CDCl<sub>3</sub>, 400 MHz) δ: 0.88–0.96 (m, 6H), 1.31–1.41 (m, 8H), 1.94–1.97 (m, 1H), 4.10–4.20 (m, 2H), 7.66 (s, 4H), 7.79 (m, *J* = 15.25 Hz, 1H), 8.25 (d, *J* = 8.00 Hz, 1H), 8.35 (s, 1H), 8.60 (d, *J* = 7.25 Hz, 1H), 8.83 (s, 1H). <sup>13</sup>C NMR (CDCl<sub>3</sub>, 125 MHz) δ: 164.46, 138.85, 138.20, 133.88, 132.36, 132.12, 131.19, 130.93, 130.28, 128.98, 127.53, 123.46, 122.80, 44.25, 38.00, 30.80, 29.71, 28.75, 10.68, 8.83. HRMS (MALDI, *m/z*) calcd for C<sub>26</sub>H<sub>26</sub>BrNO<sub>2</sub> [M+H]<sup>+</sup>, 463.1147, found 464.1220.

**2.3. Synthesis of 3.** The compound 2 (300.0 mg, 0.690 mmol) and 5-bromo-2-iodo-1,3-dimethylbenzene (300 mg, 0.965 mmol) were dissolved in a deaerated mixed solvent contains toluene (7 ml), ethanol (2 mL) and water (1 mL). After adding of the catalysts Pd(PPh<sub>3</sub>)<sub>4</sub> (79.6 mg, 0.069 mmol) and potassium carbonate (285.7 mg, 2.067 mmol), the mixture was stirred for 15 min at room temperature. Then the reaction suspension was heated to 78 °C and this reaction temperature was kept for 1 h. Following that the reaction temperature was further increased to 110 °C and stirred for 9 h. Then the reaction mixture was allowed to cool to room temperature, and extracted with chloroform, washed with water and brine. The combined organic layer was dried by anhydrous Na<sub>2</sub>SO<sub>4</sub> and concentrated by reduced pressure. The residue was purified by column chromatography (silica gel, DCM:PE = 1:4, v/v). Compound 3 was obtained as pale white solid **3** (150 mg, 60.6%). <sup>1</sup>H NMR (CDCl<sub>3</sub>, 400 MHz) δ: 0.86–0.96 (m, 6H), 1.29–1.42 (m, 8H), 1.93–1.98 (m, 1H), 2.02

(s, 6H), 4.08–4.19 (m, 2H), 7.33 (s, 2H), 7.80 (m,  $J=15.51$  Hz, 1H), 7.96 (d,  $J=1.50$  Hz, 1H), 8.20 (d,  $J=8.13$  Hz, 1H), 8.38 (d,  $J=1.50$  Hz, 1H), 8.63 (d,  $J=7.26$  Hz, 1H).  $^{13}\text{C}$  NMR ( $\text{CDCl}_3$ , 125 MHz)  $\delta$ : 164.51, 138.88, 138.23, 133.89, 132.37, 131.20, 130.31, 128.99, 127.54, 127.44, 123.48, 122.85, 44.25, 38.01, 30.81, 28.75, 24.11, 23.09, 14.11, 10.68. HRMS (MALDI,  $m/z$ ) calcd for  $\text{C}_{28}\text{H}_{30}\text{BrNO}_2$   $[\text{M}+\text{H}]^+$ , 491.1460, found 492.1533.

### 3. Molecular structure characterization data

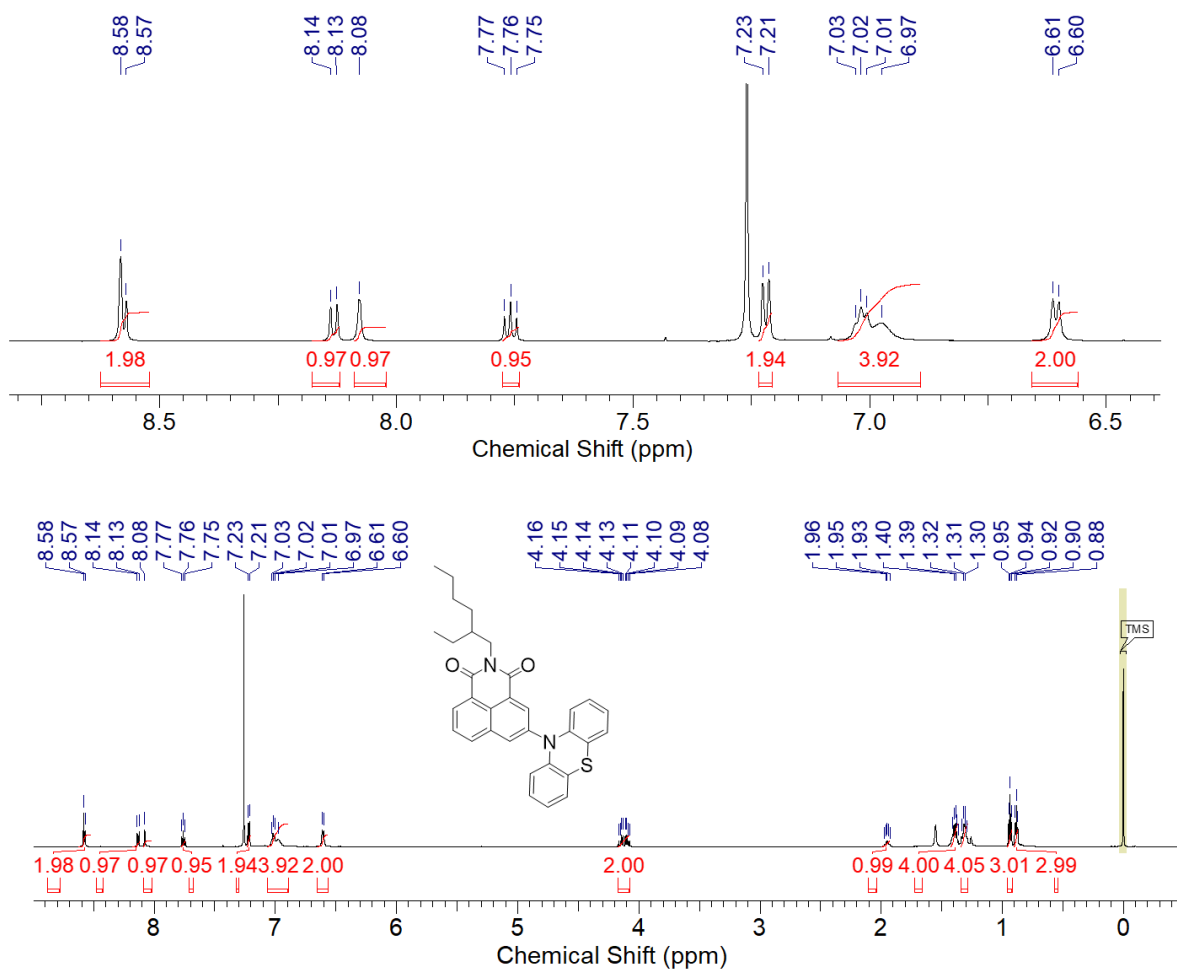


Figure S1. <sup>1</sup>H NMR spectrum of NI-PTZ in CDCl<sub>3</sub> (400 MHz), 25 °C.

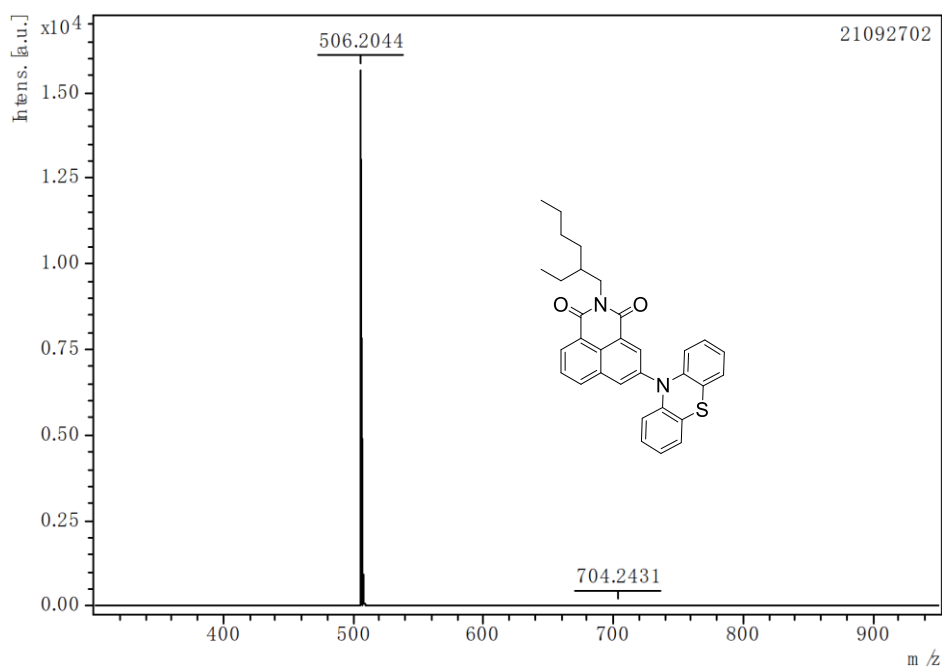


Figure S2. MALDI-HRMS spectrum of NI-PTZ, 25 °C.

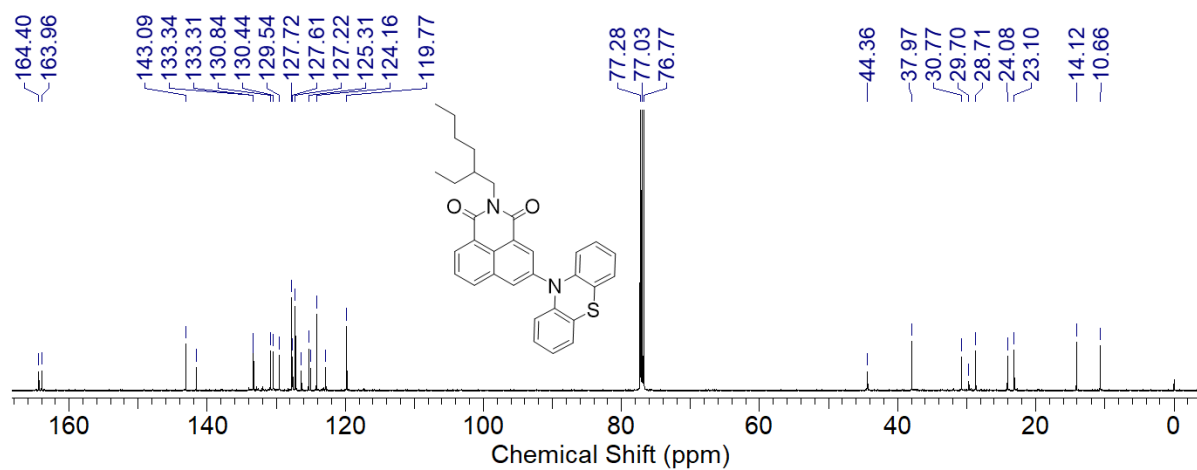


Figure S3.  $^{13}\text{C}$  NMR spectrum of NI-PTZ in  $\text{CDCl}_3$  (125 MHz), 25 °C.

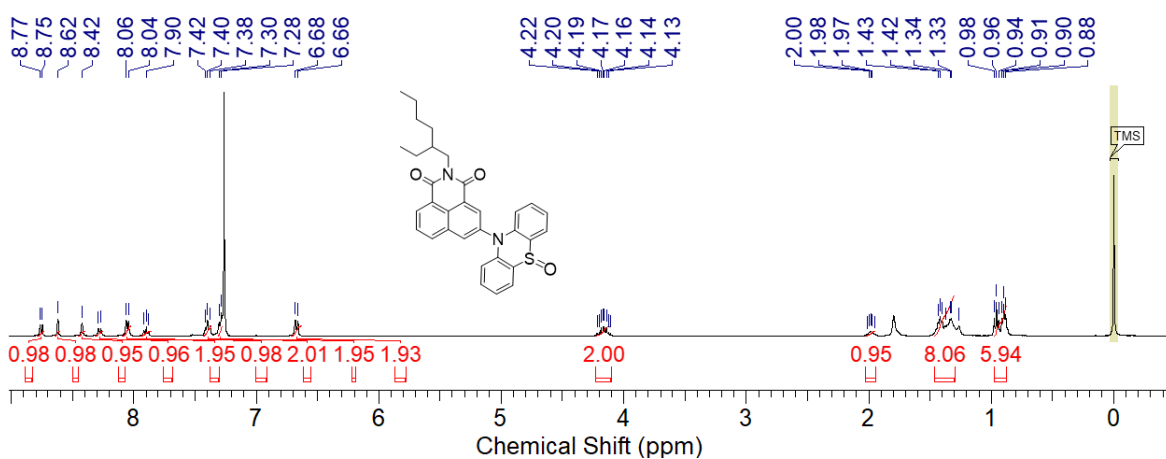
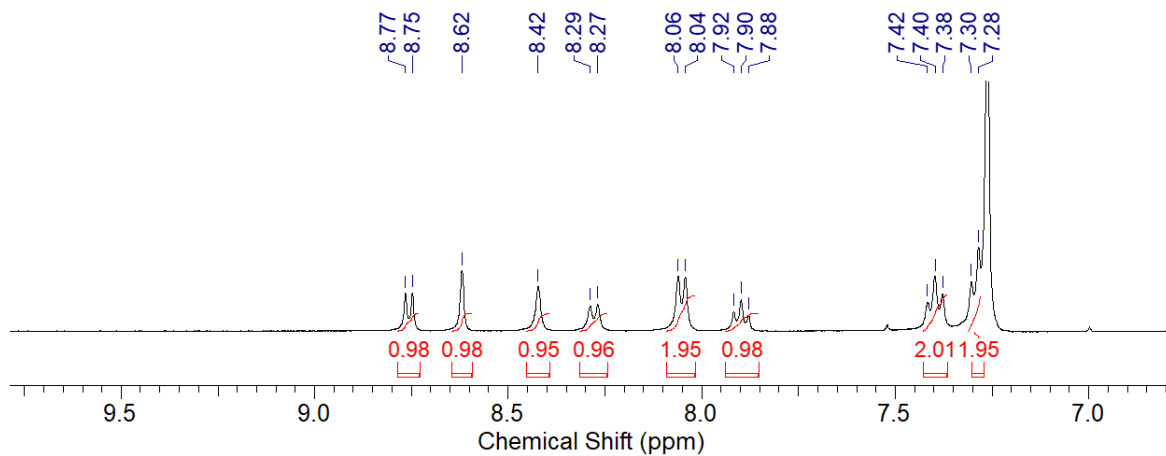


Figure S4. <sup>1</sup>H NMR spectrum of NI-PTZ-O in CDCl<sub>3</sub> (400 MHz), 25 °C.



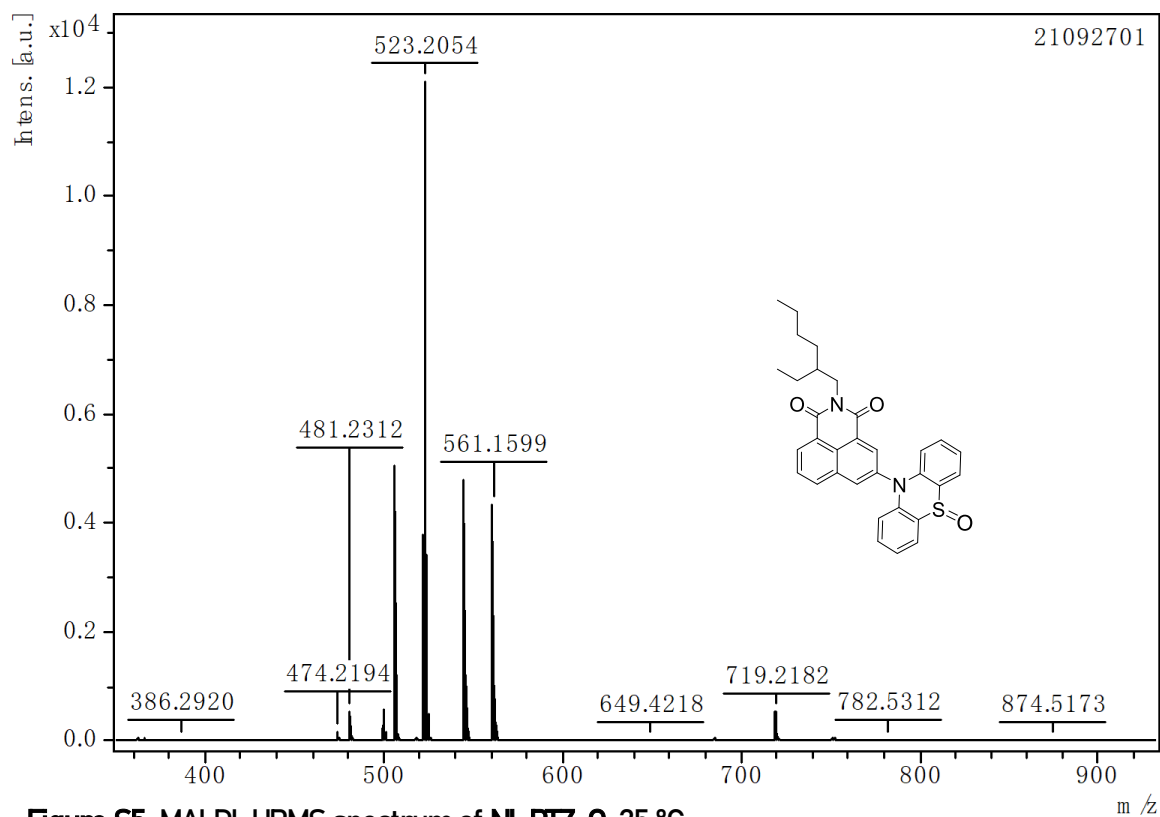


Figure S5. MALDI-HRMS spectrum of NI-PTZ-O, 25 °C.

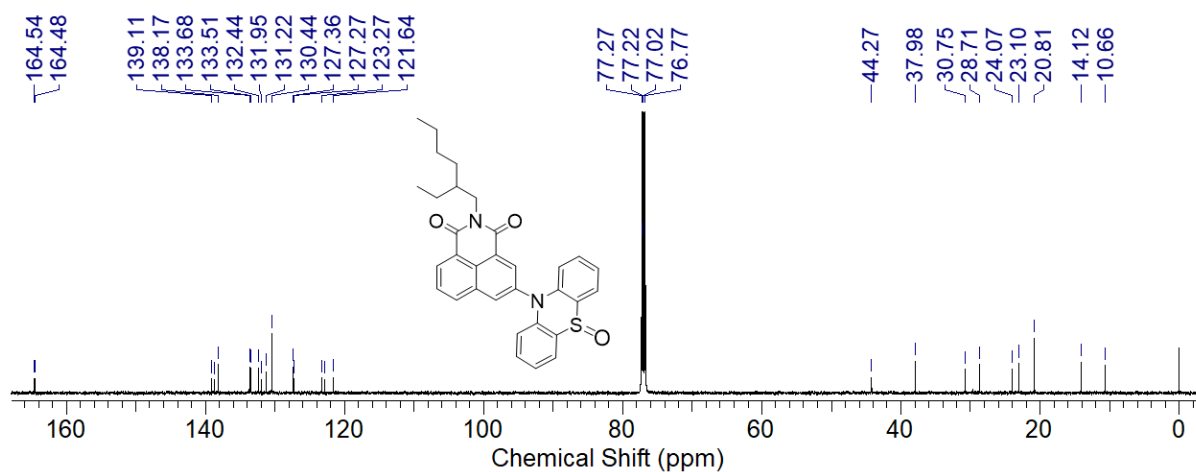


Figure S6. <sup>13</sup>C NMR spectrum of NI-PTZ-O in CDCl<sub>3</sub> (125 MHz), 25 °C.

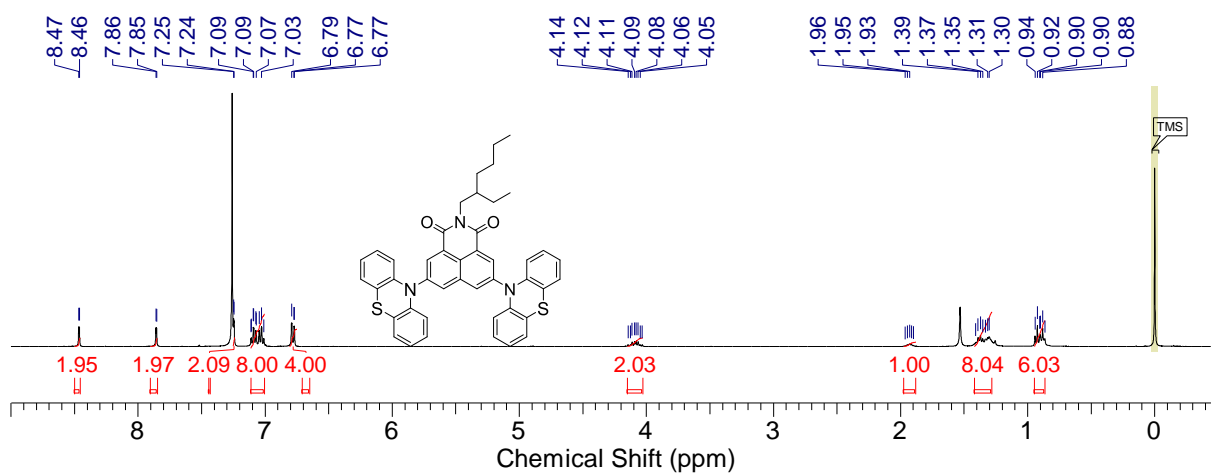
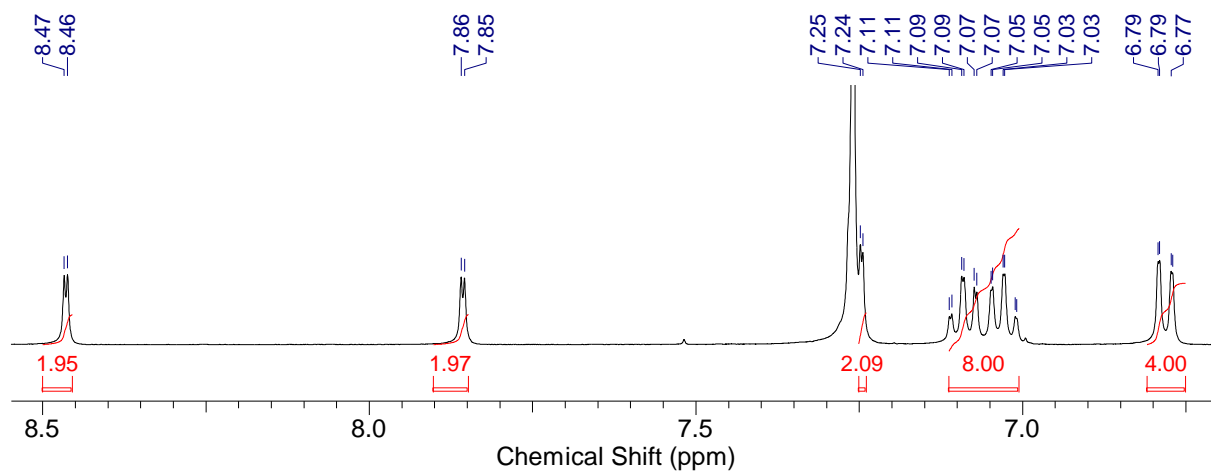
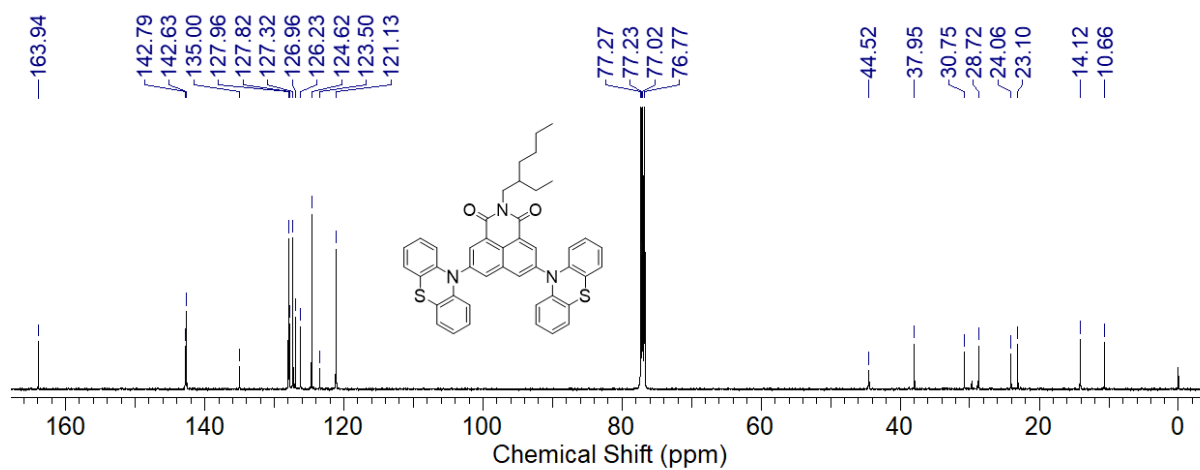
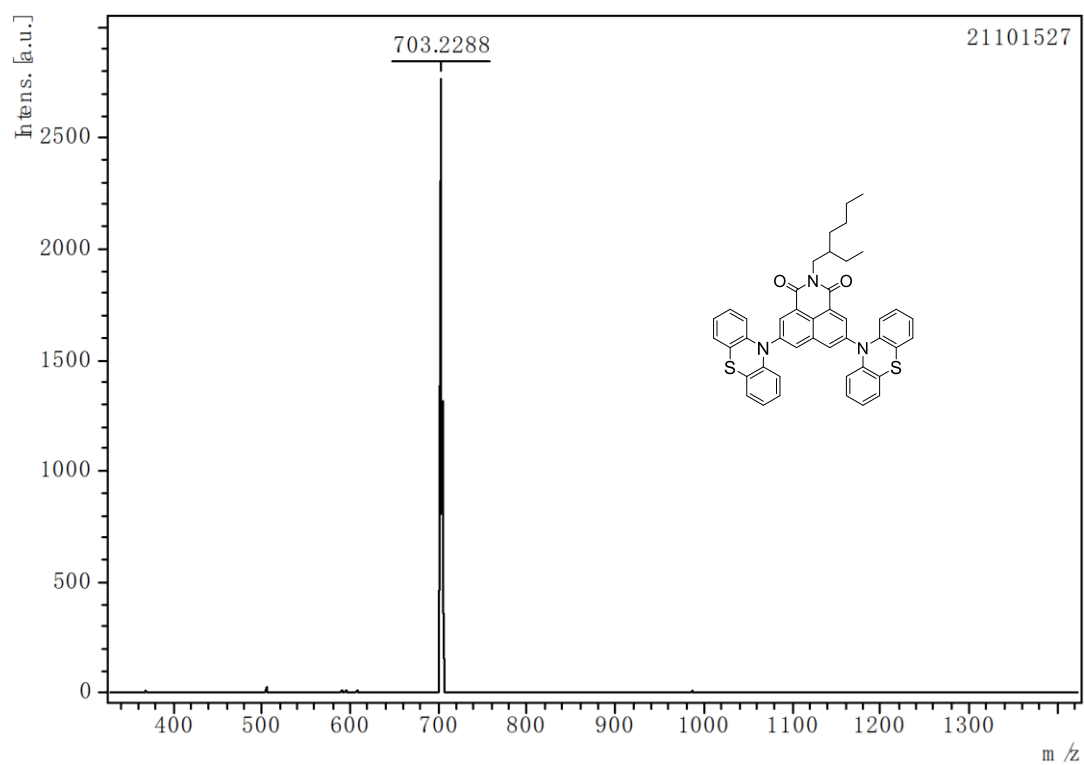


Figure S7.  $^1\text{H}$  NMR spectrum of NI-PTZ<sub>2</sub> in  $\text{CDCl}_3$  (400 MHz), 25 °C.



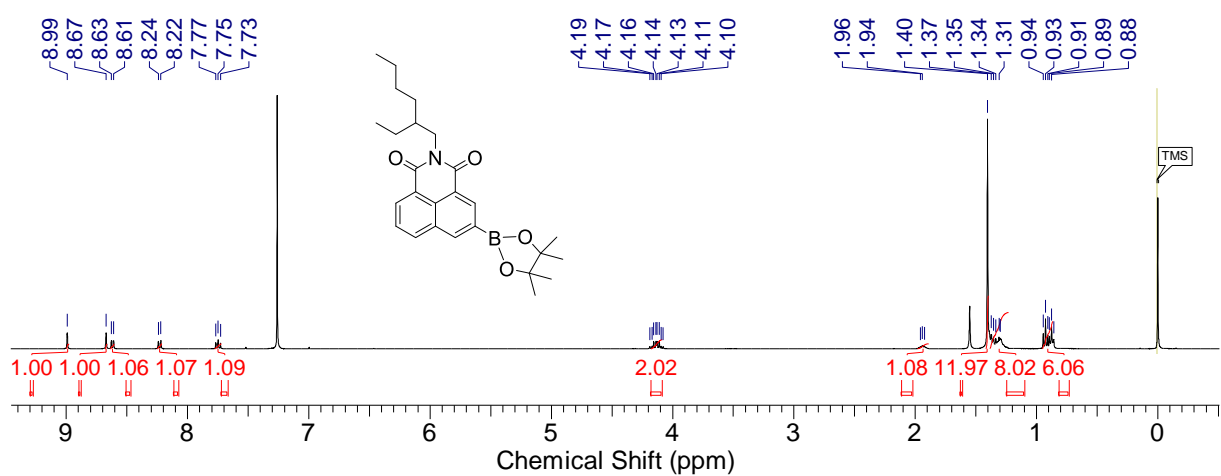
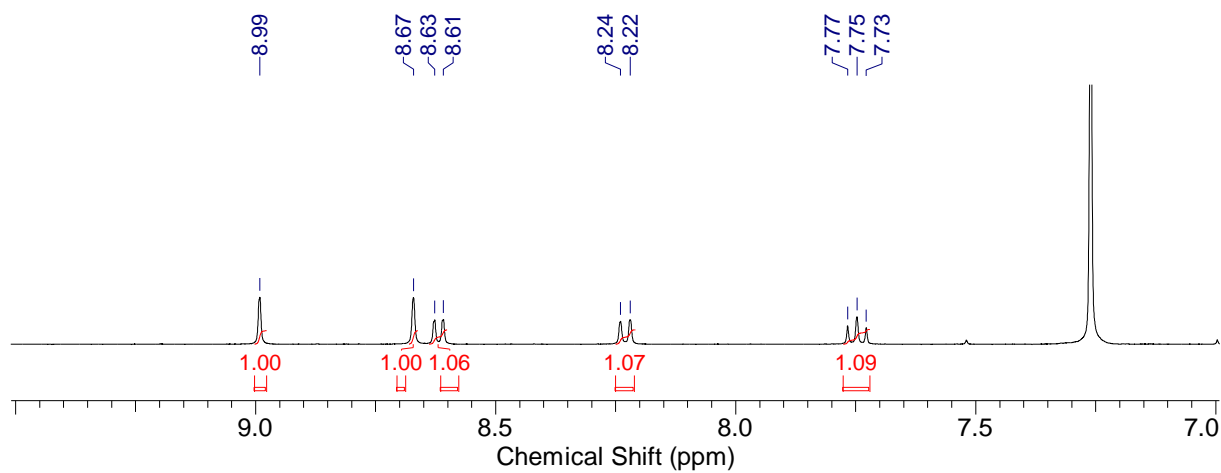


Figure S10.  $^1\text{H}$  NMR spectrum of **2** in  $\text{CDCl}_3$  (400 MHz), 25  $^\circ\text{C}$ .

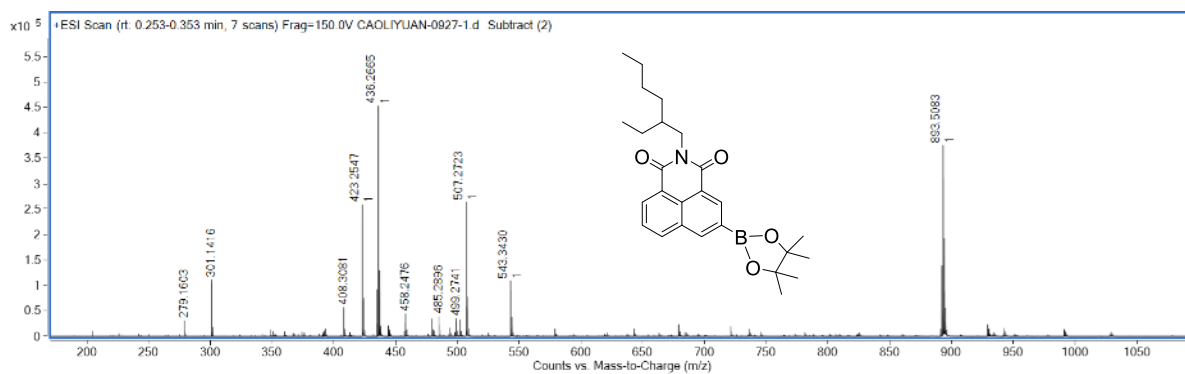


Figure S11. ESI-HRMS spectrum of **2**, 25  $^\circ\text{C}$ .

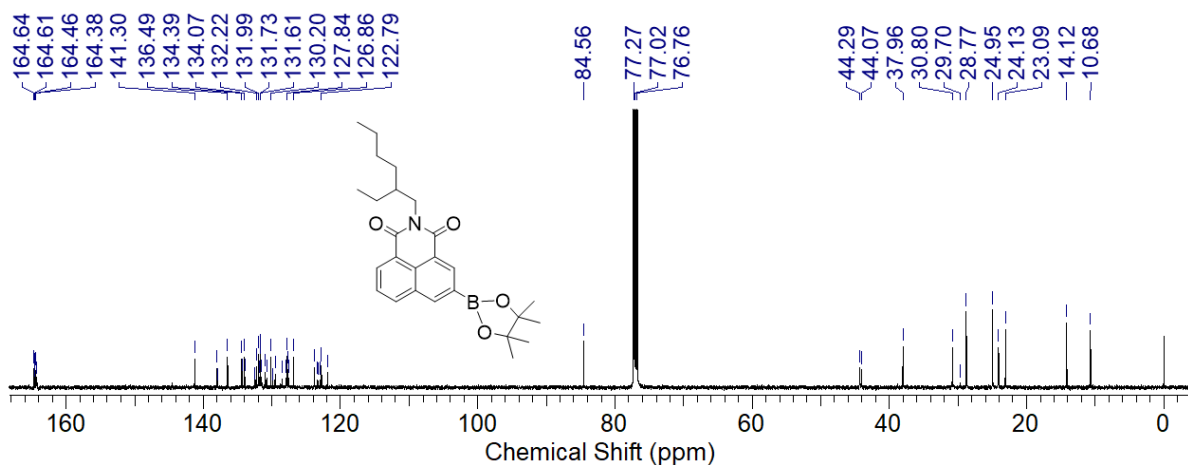


Figure S12. <sup>13</sup>C NMR spectrum of **2** in CDCl<sub>3</sub> (125 MHz), 25 °C.

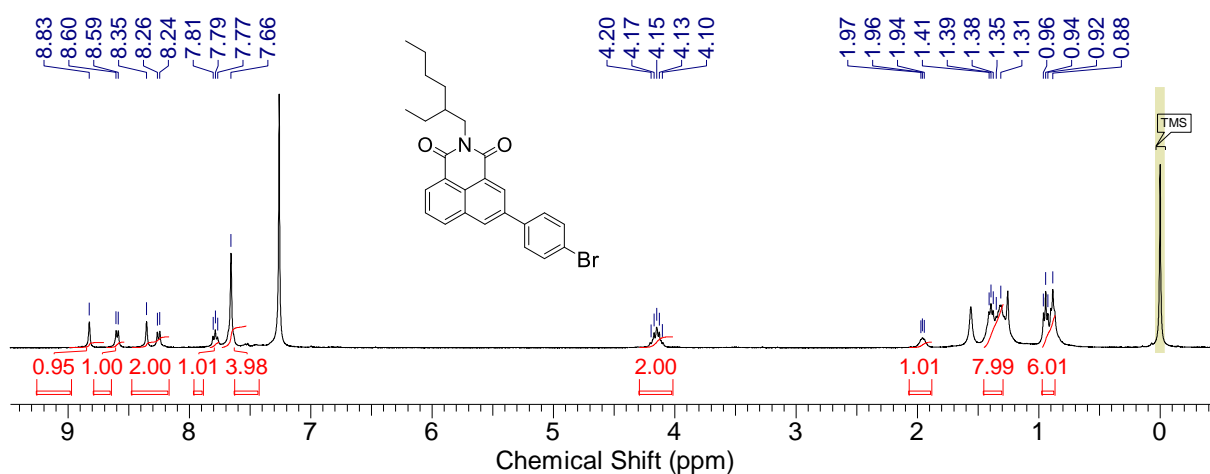
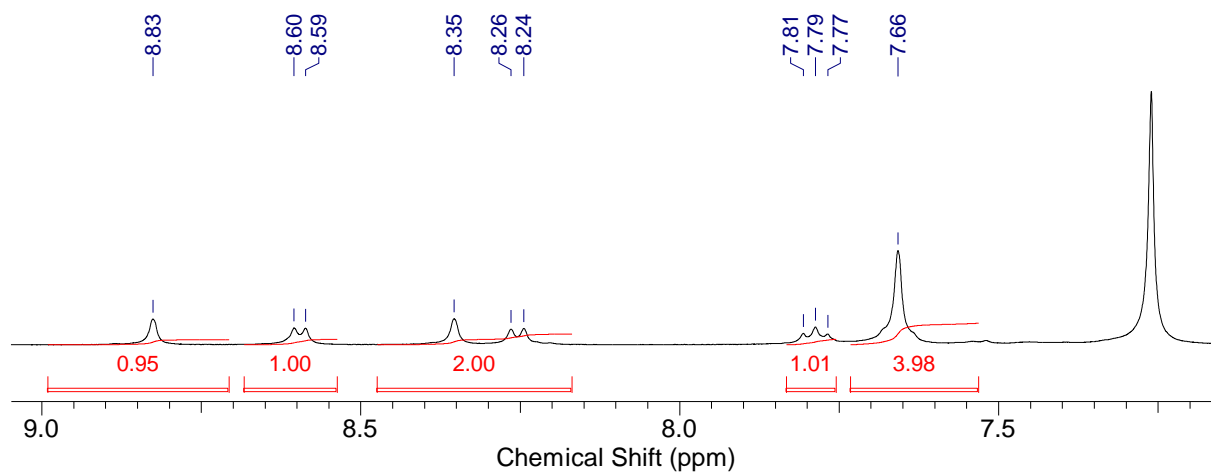


Figure S13. <sup>1</sup>H NMR spectrum of NI-Ph-Br in CDCl<sub>3</sub> (400 MHz), 25 °C.

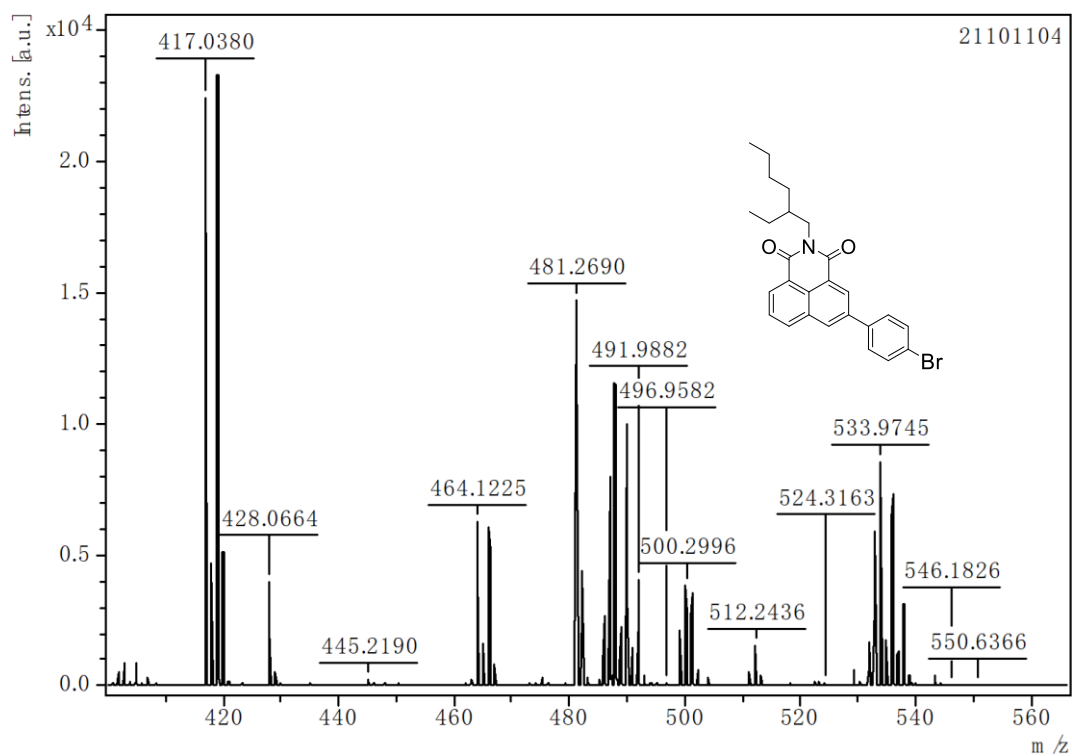


Figure S14. MALDI-HRMS spectrum of NI-Ph-Br, 25 °C.

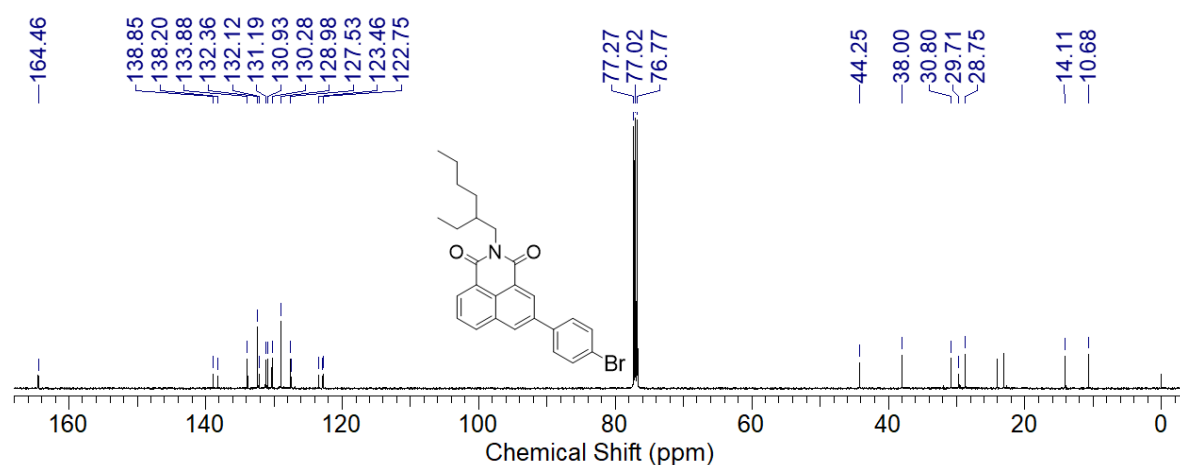


Figure S15. <sup>13</sup>C NMR spectrum of NI-Ph-Br in CDCl<sub>3</sub> (125 MHz), 25 °C.

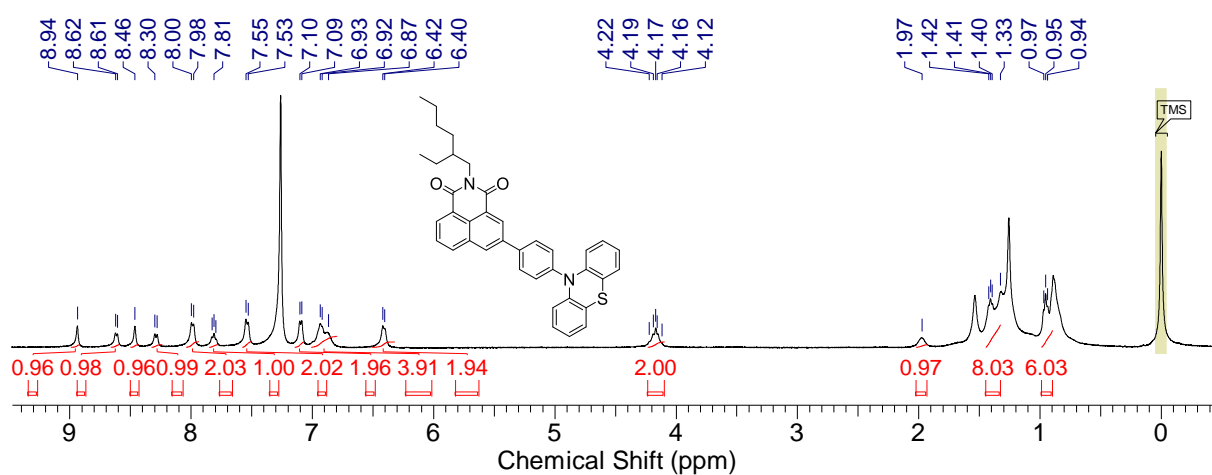
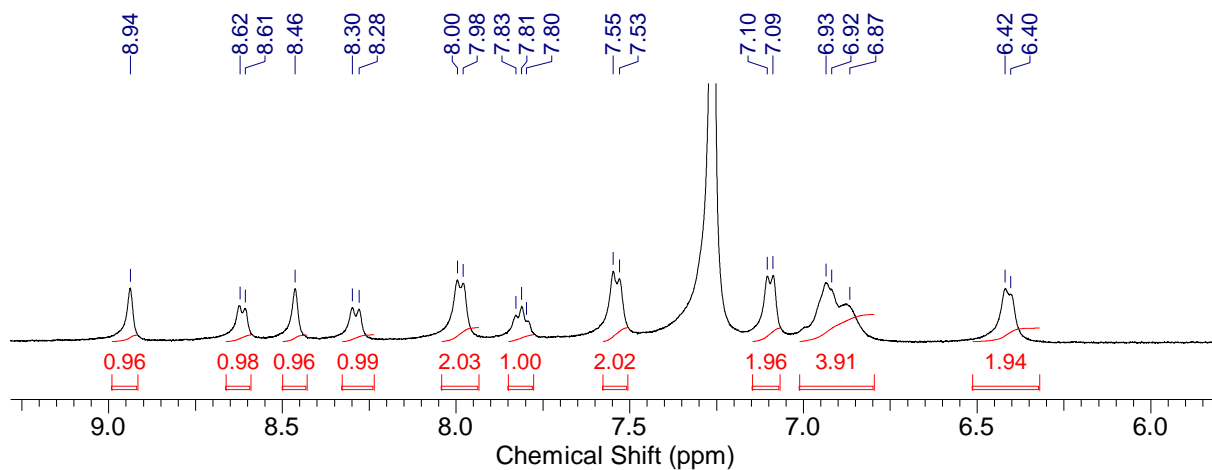


Figure S16.  $^1\text{H}$  NMR spectrum of NI-Ph-PTZ in  $\text{CDCl}_3$  (400 MHz), 25  $^\circ\text{C}$ .

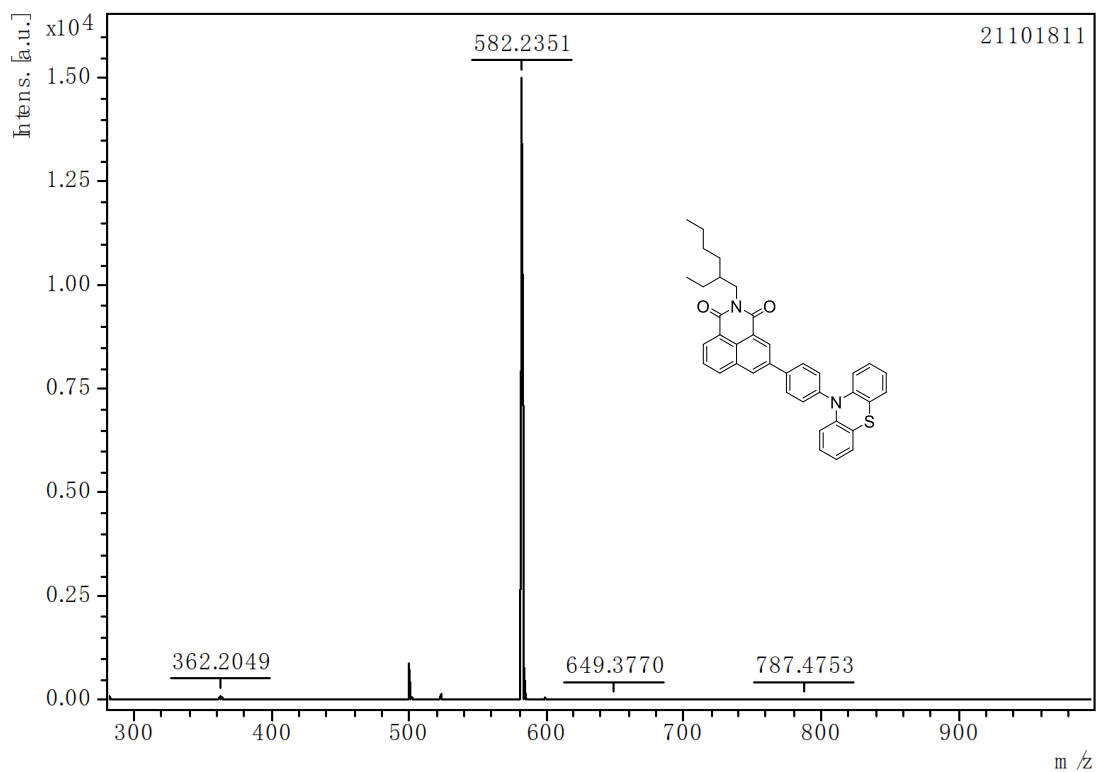


Figure S17. MALDI-HRMS spectrum of NI-Ph-PTZ, 25 °C.

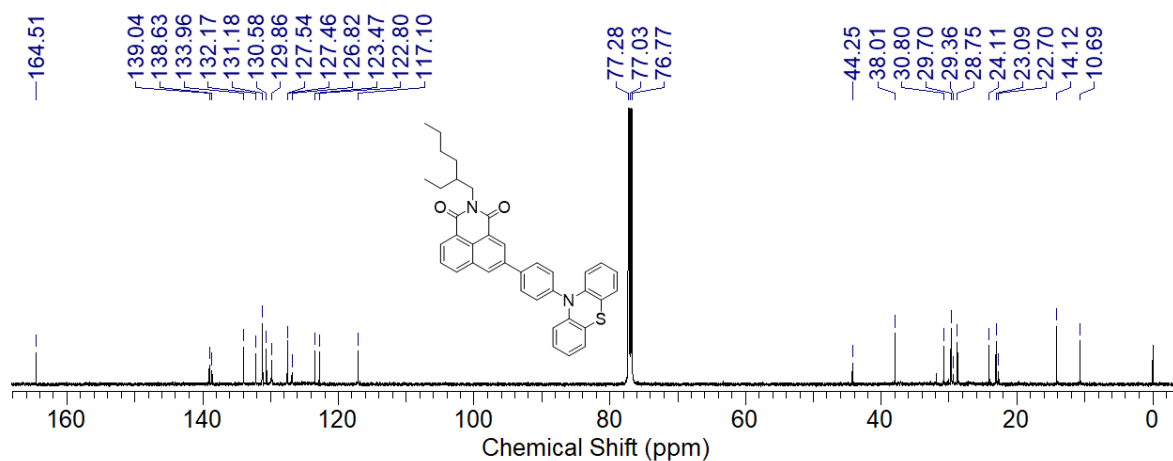


Figure S18.  $^{13}\text{C}$  NMR spectrum of NI-Ph-PTZ in  $\text{CDCl}_3$  (125 MHz), 25 °C.



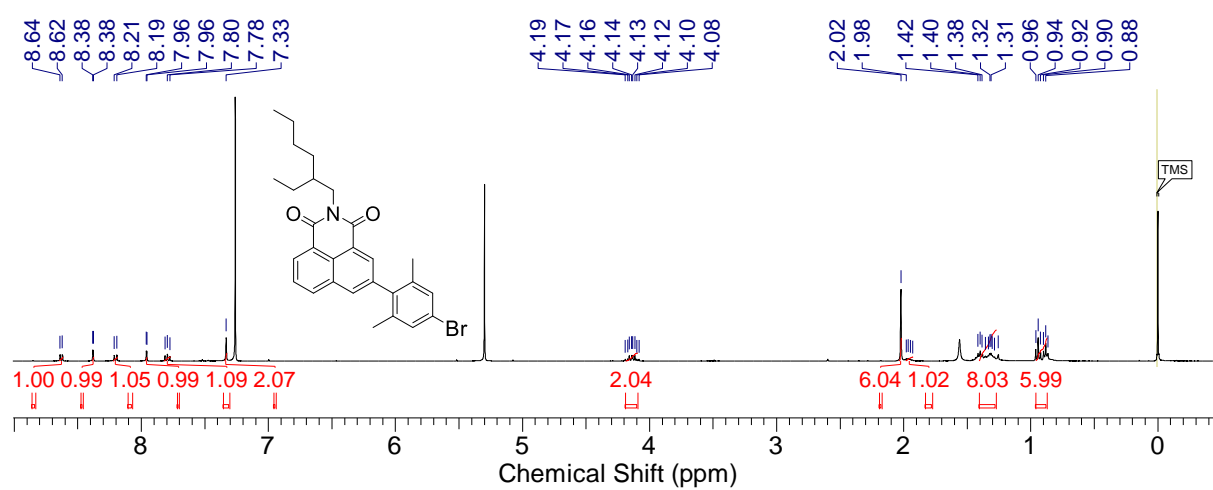
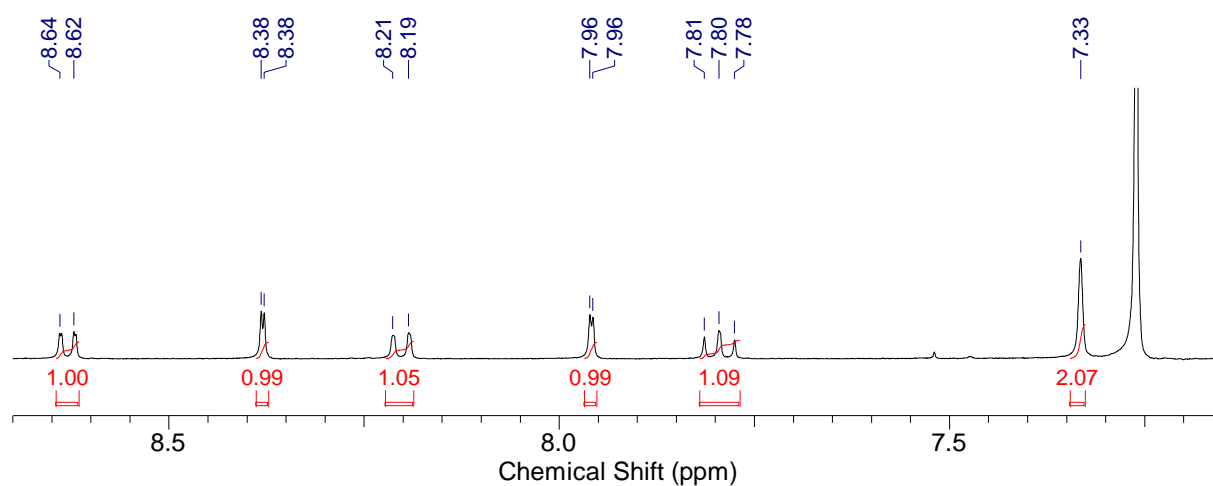


Figure S19.  $^1\text{H}$  NMR spectrum of **3** in  $\text{CDCl}_3$  (400 MHz), 25 °C.

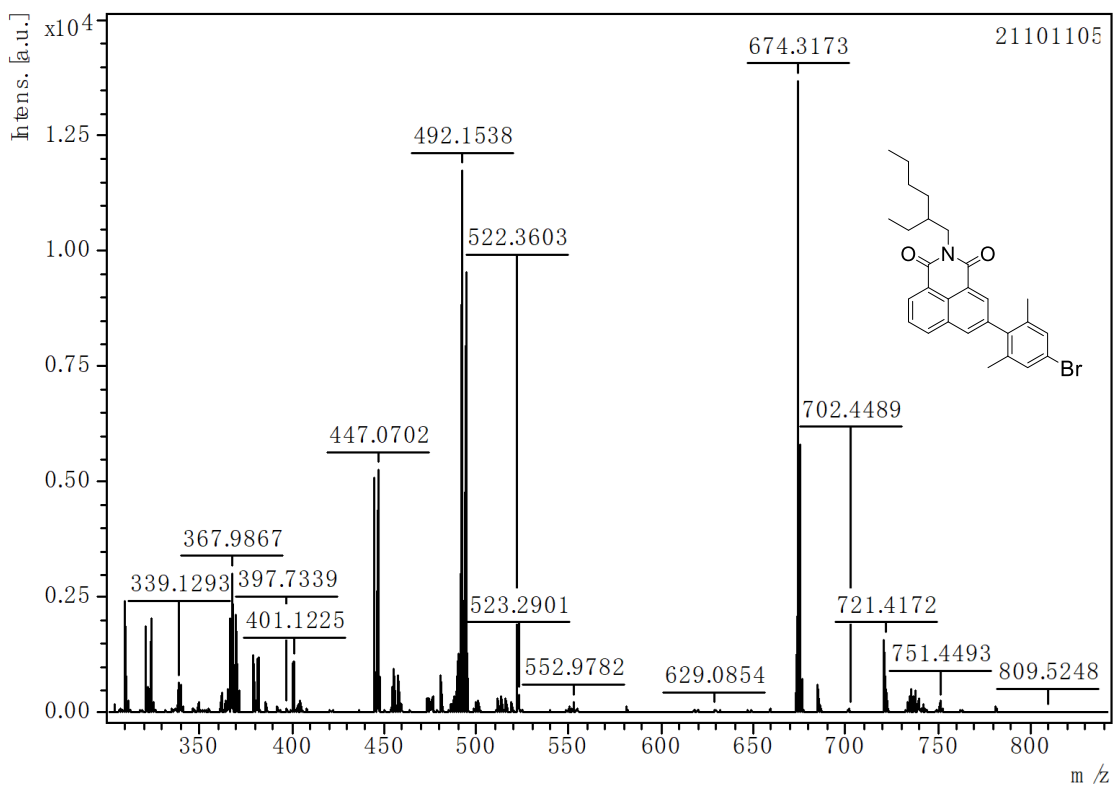


Figure S20. MALDI-HRMS spectrum of 3, 25 °C.

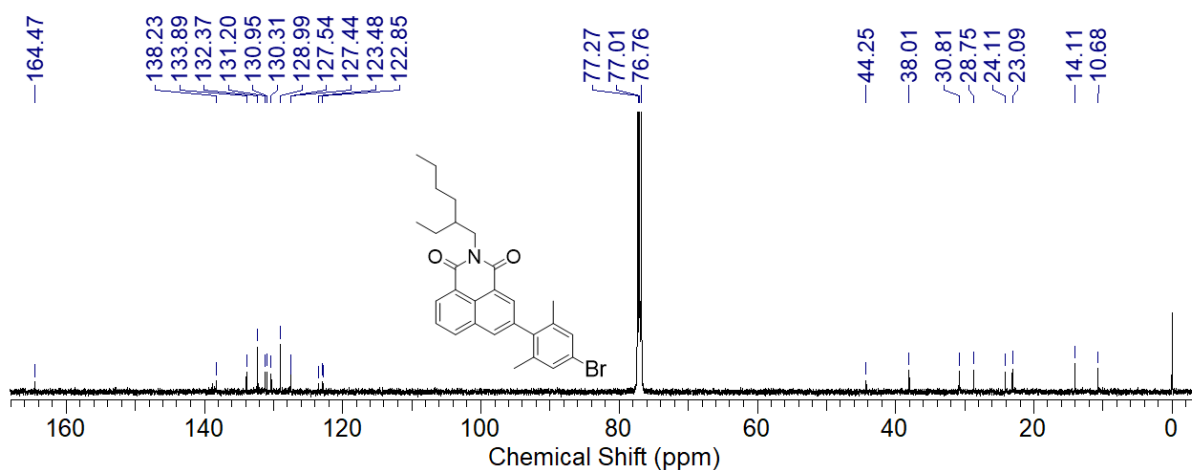


Figure S21. <sup>13</sup>C NMR spectrum of 3 in CDCl<sub>3</sub> (125 MHz), 25 °C.

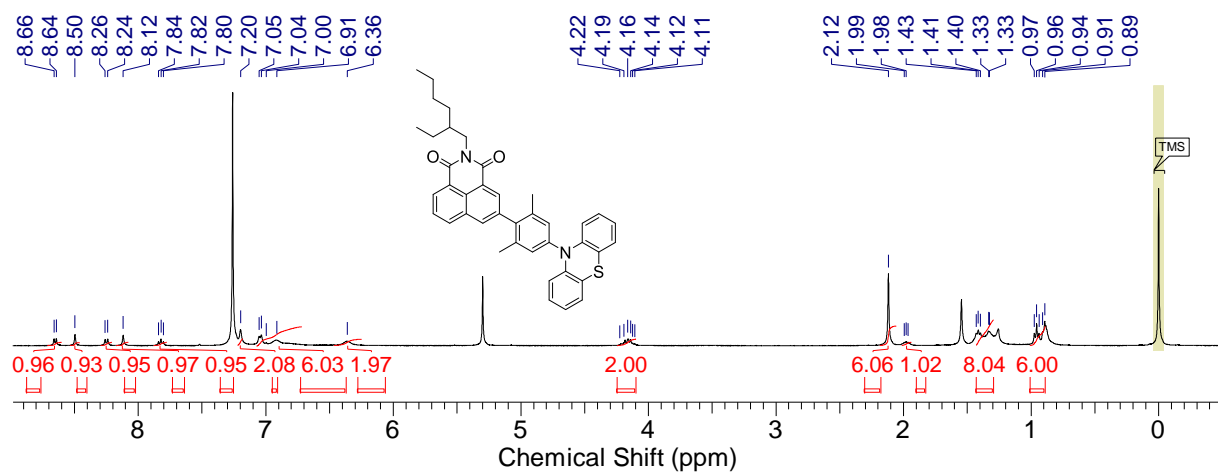
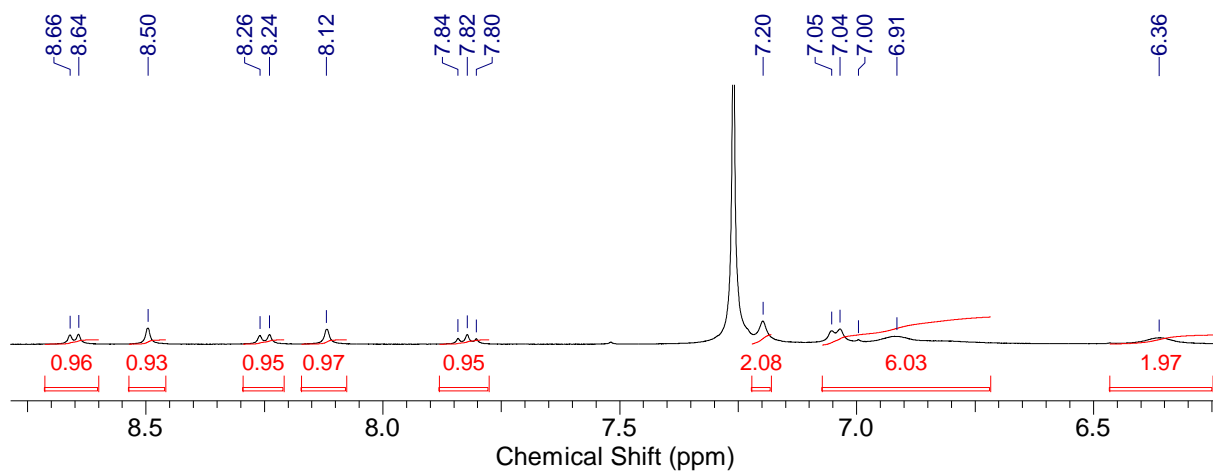


Figure S22.  $^1\text{H}$  NMR spectrum of NI-PhMe<sub>2</sub>-PTZ in  $\text{CDCl}_3$  (400 MHz), 25 °C.

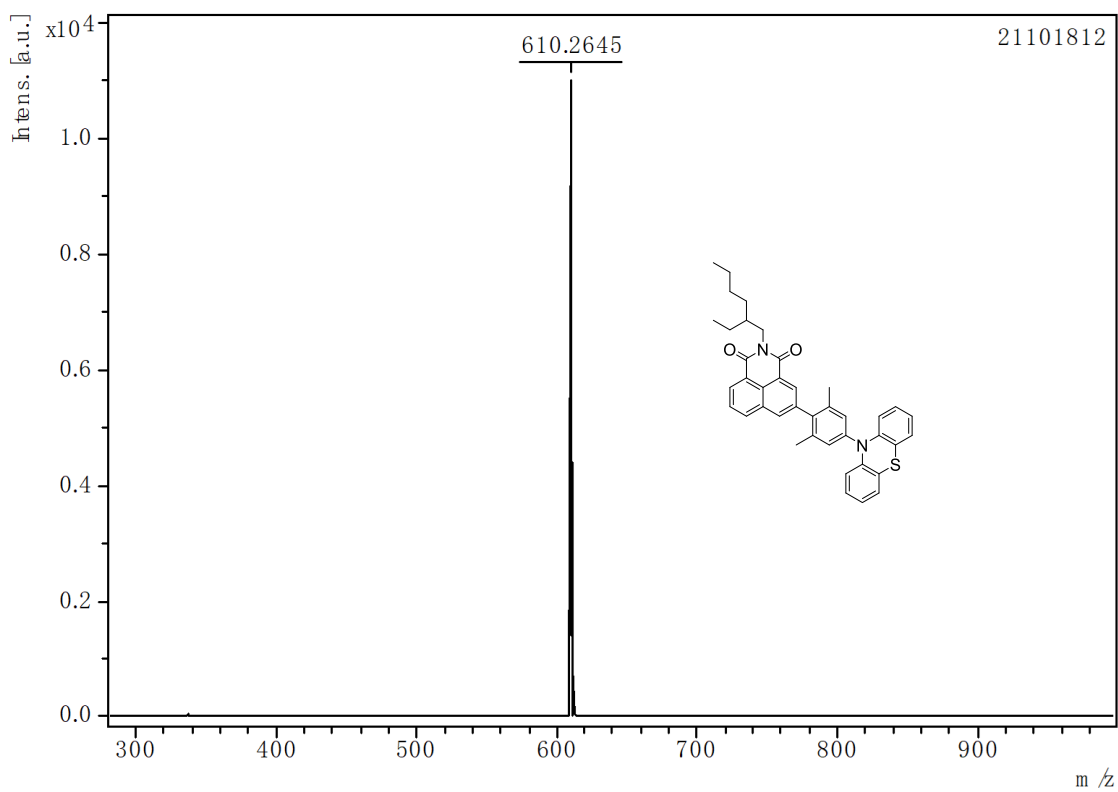


Figure S23. MALDI-MS spectrum of NI-PhMe<sub>2</sub>-PTZ, 25 °C.

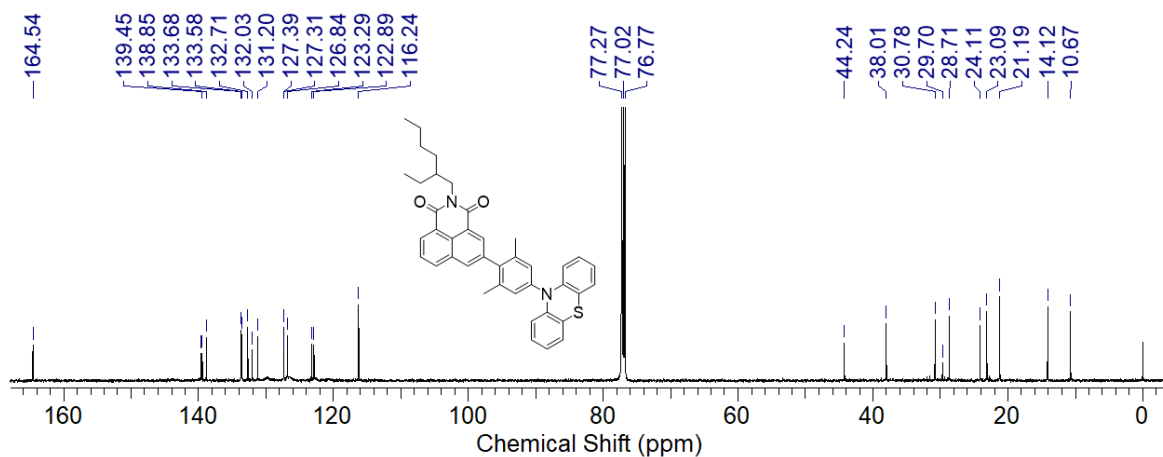
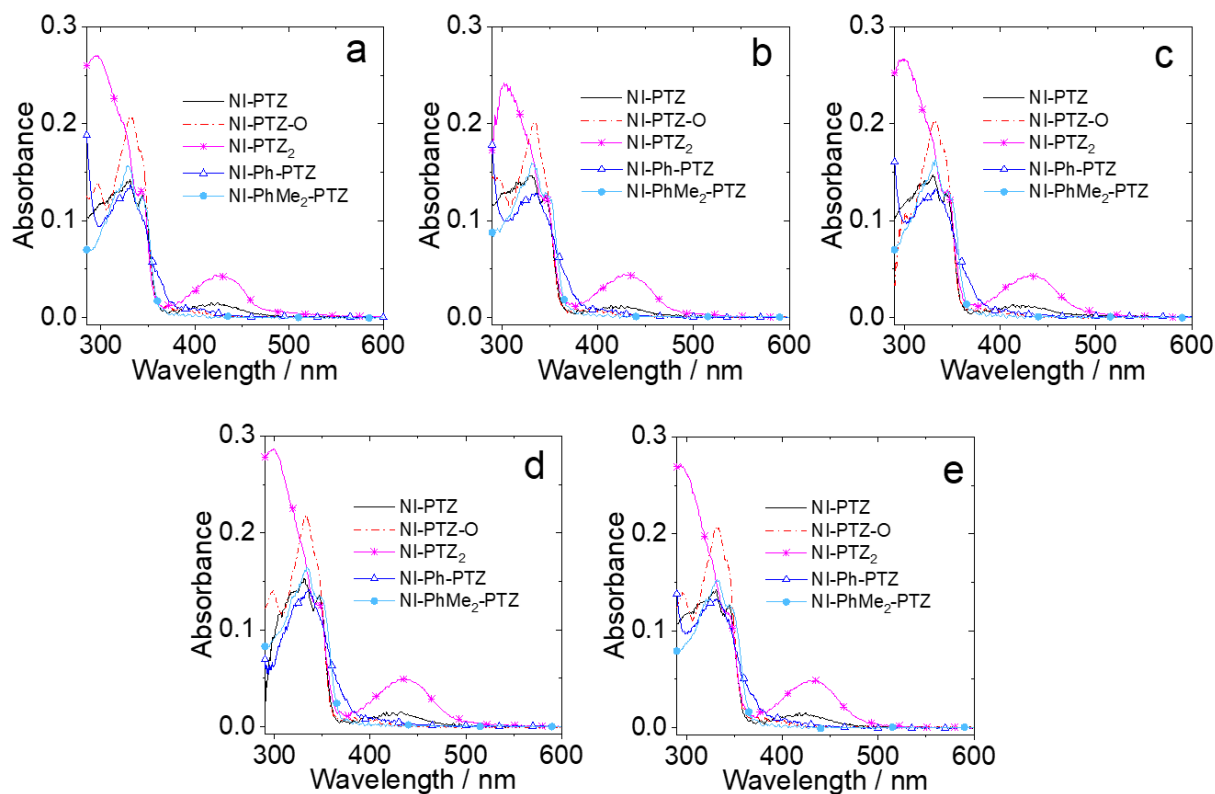
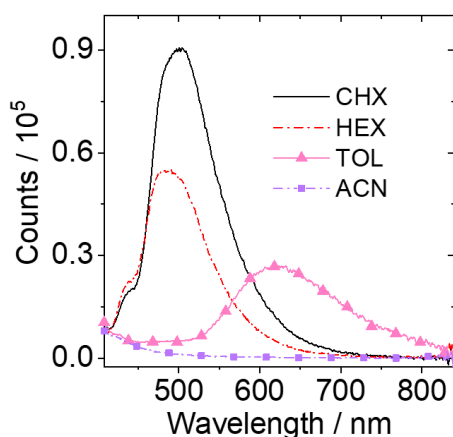


Figure S24. <sup>13</sup>C NMR spectrum of NI-PhMe<sub>2</sub>-PTZ in CDCl<sub>3</sub> (125 MHz), 25 °C.

## 4. Steady state UV-vis absorption and luminescence spectra



**Figure S25.** UV-vis absorption spectra of NI-PTZ; NI-PTZ-O; NI-PTZ<sub>2</sub>; NI-Ph-PTZ and NI-PhMe<sub>2</sub>-PTZ in (a) cyclohexane (CHX); (b) toluene (TOL); (c) tetrahydrofuran (THF); (d) dichloromethane (DCM); (e) acetonitrile (ACN).  $c = 1.0 \times 10^{-5}$  M, 20 °C.



**Figure S26.** Fluorescence emission spectra of **Ni-PhMe<sub>2</sub>-PTZ** in different solvents.  $A = 0.146$ ,  $\lambda_{\text{ex}} = 330 \text{ nm}$ ,  $20 \text{ }^\circ\text{C}$ .

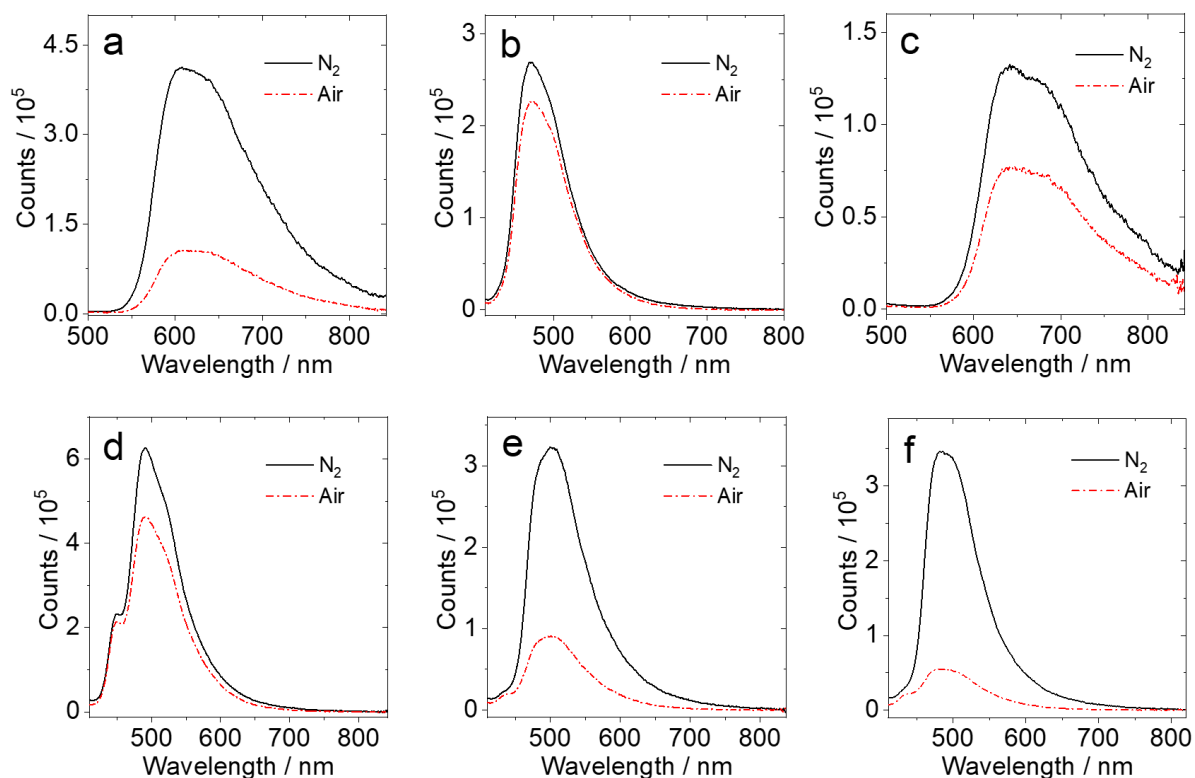


**Figure S27.** Fluorescence emission spectra of (a) **Ni-PTZ**; (b) **Ni-PTZ-O**; (c) **Ni-PTZ<sub>2</sub>**; (d) **Ni-Ph-PTZ**; (e) **Ni-PhMe<sub>2</sub>-PTZ** in **CYC** and (f) **Ni-PhMe<sub>2</sub>-PTZ** in *n*-**HEX**. Under different atmospheres (**N<sub>2</sub>**, **air**).  $A = 0.146$ ,  $\lambda_{\text{ex}} = 330 \text{ nm}$ ,  $20 \text{ }^\circ\text{C}$ .

## 5. Fluorescence lifetimes

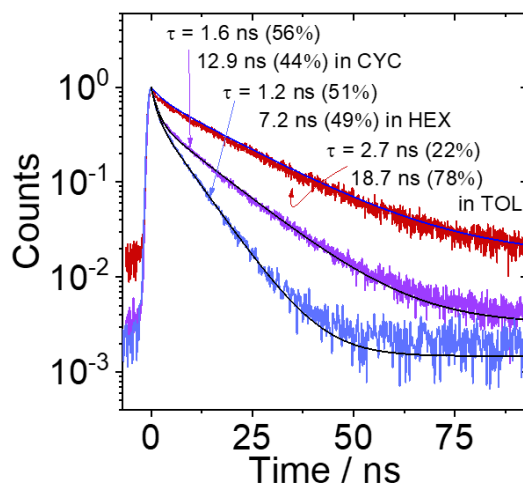


**Figure S28.** Decay traces of the luminescence of **Ni-PhMe<sub>2</sub>-PTZ** in different solvents. Excited with picoseconds pulsed laser for fluorescence band ( $\lambda_{\text{ex}} = 479 \text{ nm}$ ),  $c = 1.0 \times 10^{-5} \text{ M}$ ,  $20 \text{ }^\circ\text{C}$ .

## 6. Phosphorescence spectra

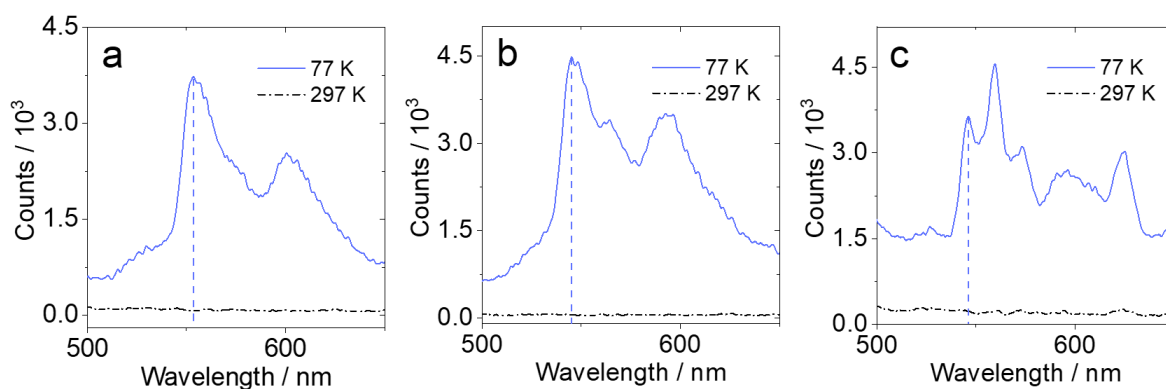


**Figure S29.** Phosphorescence spectra of the compounds (a) **Ni-Ph-PTZ** ( $\lambda_{\text{ex}} = 554 \text{ nm}$ ); (b) **Ni-PhMe<sub>2</sub>-PTZ** ( $\lambda_{\text{ex}} = 545 \text{ nm}$ ); (c) **Ni-3BR** ( $\lambda_{\text{ex}} = 547 \text{ nm}$ ) at  $77 \text{ K}$ , in 2-Methyltetrahydrofuran,  $c = 1.0 \times 10^{-5} \text{ M}$ .

## 7. Phosphorescence lifetimes

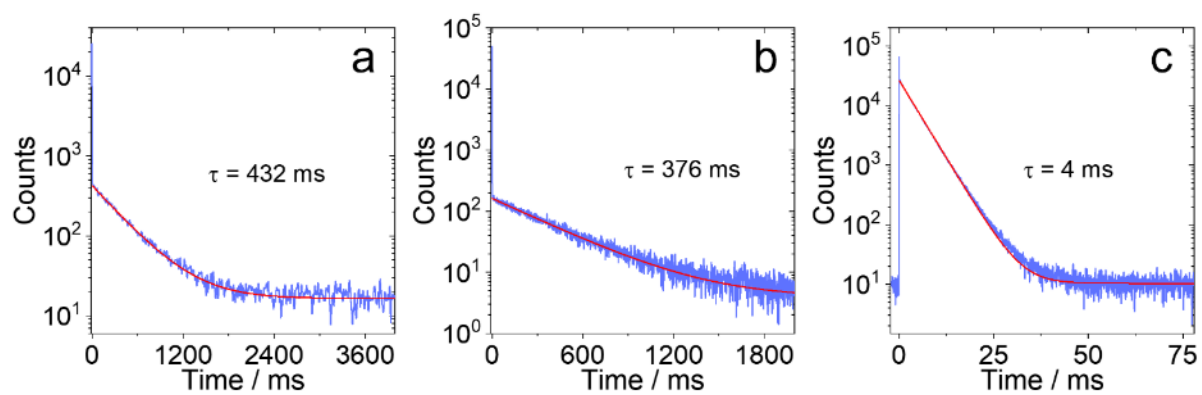


**Figure S30.** Decay traces of the phosphorescence of the compounds (a) NI-Ph-PTZ ( $\lambda_{\text{ex}} = 554 \text{ nm}$ ); (b) NI-PhMe<sub>2</sub>-PTZ ( $\lambda_{\text{ex}} = 545 \text{ nm}$ ) and (c) NI-3Br ( $\lambda_{\text{ex}} = 547 \text{ nm}$ ) in 2-Methyltetrahydrofuran,  $c = 1.0 \times 10^{-5} \text{ M}$ , 77 K.



## 8. Spectroelectrochemistry measurement

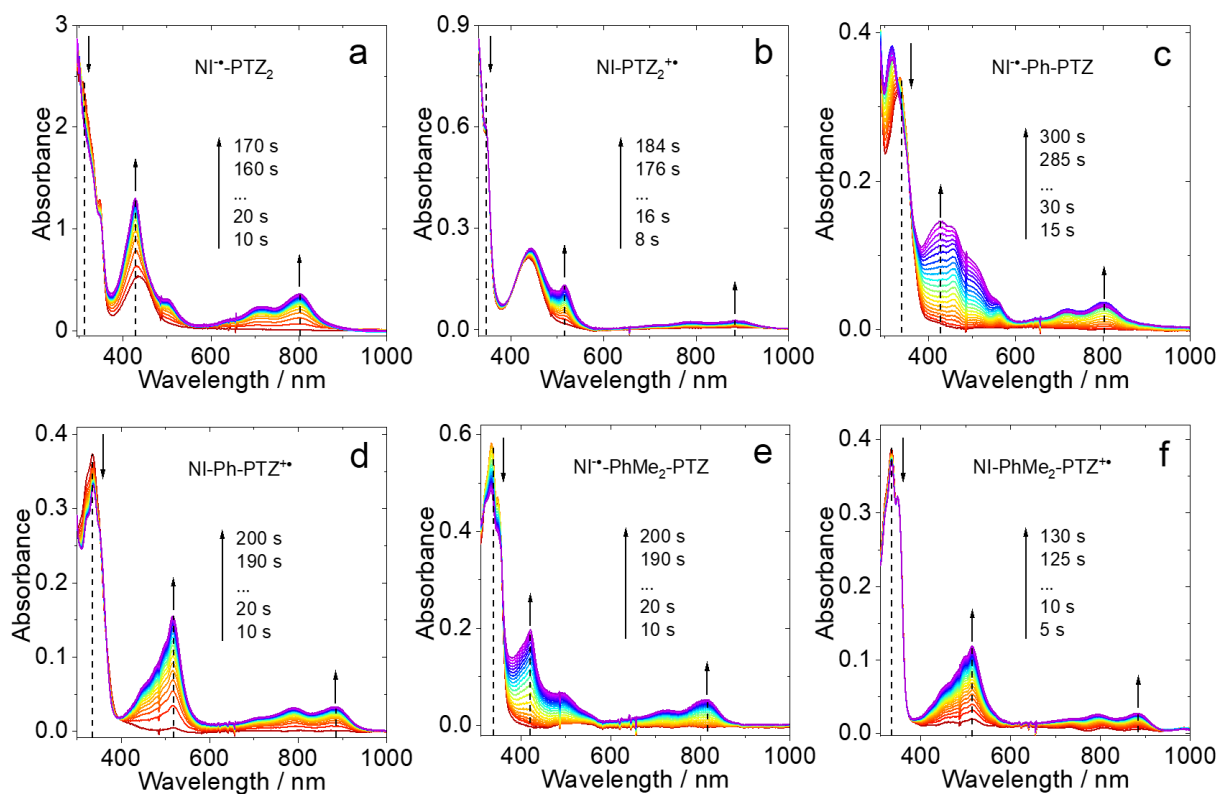


**Figure S31.** Spectroelectrochemistry traces of the UV-vis absorption spectra for (a) **Ni-PTZ<sub>2</sub>** observed from neutral (red) to monoanion (purple) at controlled-potential of  $-1.83$  V (vs. Ag/AgNO<sub>3</sub>); (b) **Ni-PTZ<sub>2</sub>** observed from neutral (red) to monocationic (purple) at controlled-potential of  $0.53$  V (vs. Ag/AgNO<sub>3</sub>); (c) **Ni-Ph-PTZ** observed from neutral (red) to monoanion (purple) at controlled-potential of  $-1.85$  V (vs. Ag/AgNO<sub>3</sub>); (d) **Ni-Ph-PTZ** observed from neutral (red) to monocationic (purple) at controlled-potential of  $0.55$  V (vs. Ag/AgNO<sub>3</sub>); (e) **Ni-PhMe<sub>2</sub>-PTZ** observed from neutral (red) to monoanion (purple) at controlled-potential of  $-1.85$  V (vs. Ag/AgNO<sub>3</sub>); (f) **Ni-PhMe<sub>2</sub>-PTZ** observed from neutral (red) to monocationic (purple) at controlled-potential of  $0.60$  V (vs. Ag/AgNO<sub>3</sub>). In deaerated dichloromethane containing  $0.10$  M Bu<sub>4</sub>[NPF<sub>6</sub>] as supporting electrolyte and with Ag/AgNO<sub>3</sub> as reference electrode,  $20$  °C.

## 9. Nanosecond transient absorption spectroscopy

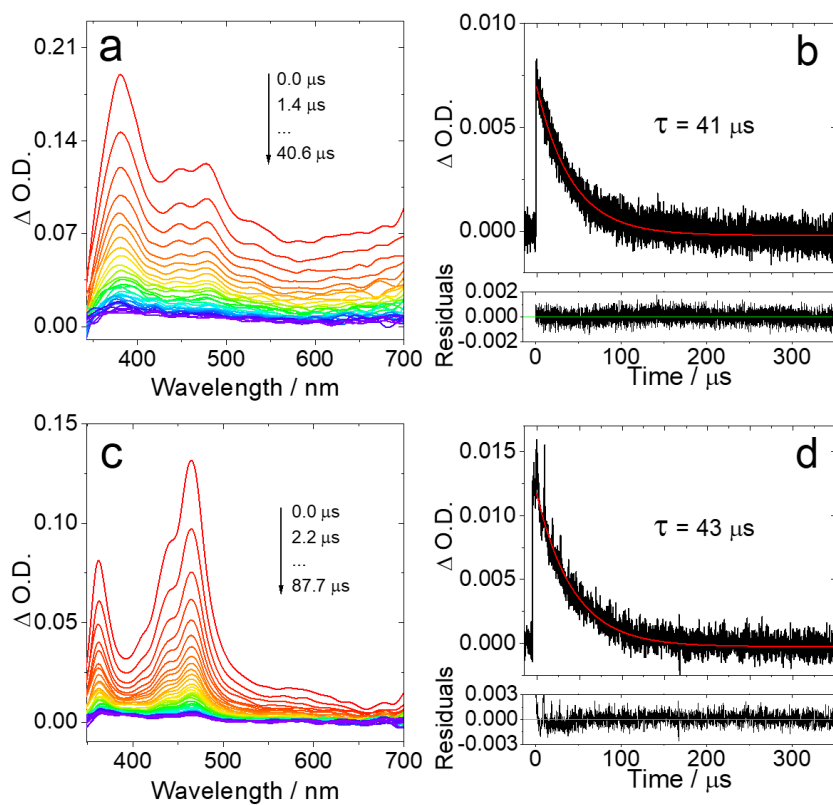


**Figure S32.** Nanosecond transient absorption of (a) Ni-Ph-PTZ ( $c = 5 \times 10^{-5} M$ ) and (c) Ni-PhMe<sub>2</sub>-PTZ ( $c = 5 \times 10^{-5} M$ ). Decay traces of (b) Ni-Ph-PTZ ( $c = 2 \times 10^{-6} M$ ) at 380 nm and (d) Ni-PhMe<sub>2</sub>-PTZ ( $c = 2 \times 10^{-6} M$ ). In deaerated HEX,  $\lambda_{ex} = 355$  nm, 20 °C.

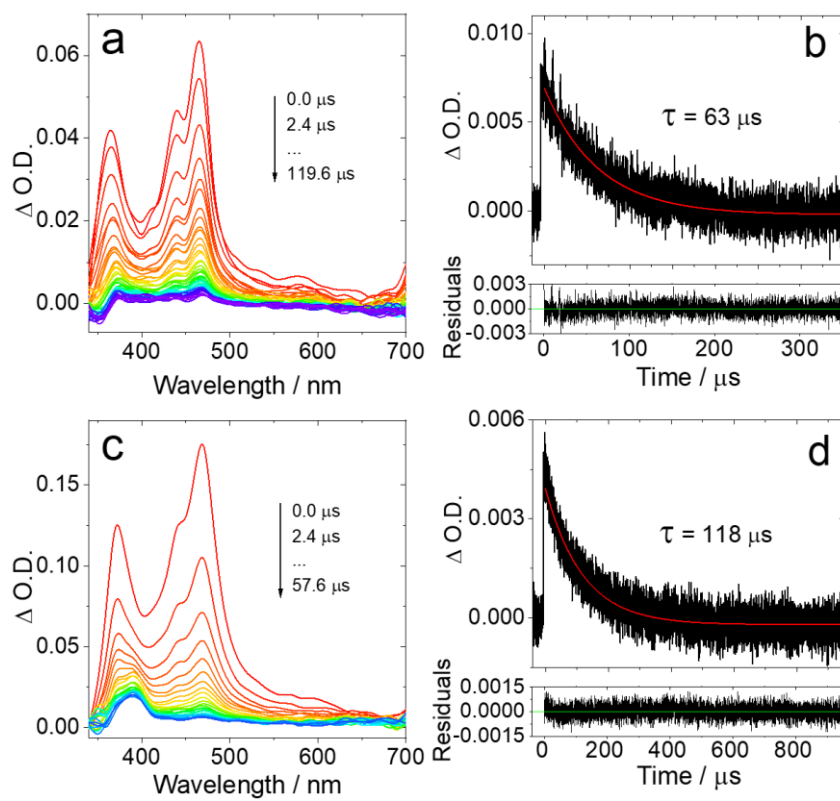


**Figure S33.** Nanosecond transient absorption of **Ni-3Br** (a)  $c = 3.0 \times 10^{-5} \text{ M}$  in deaerated HEX and (c)  $c = 1.0 \times 10^{-4} \text{ M}$  in deaerated ACN. Decay traces of (b)  $c = 2.0 \times 10^{-6} \text{ M}$  in deaerated HEX and (d)  $c = 1.0 \times 10^{-6} \text{ M}$  in deaerated ACN at 470 nm.  $\lambda_{\text{ex}} = 355 \text{ nm}$ , 20 °C.

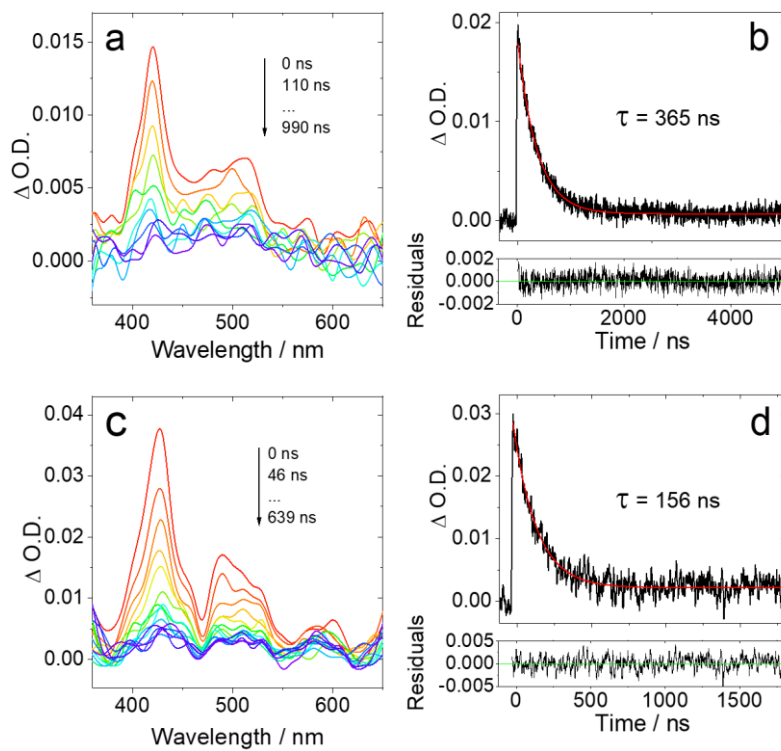


**Figure S34.** Nanosecond transient absorption of (a) NI-PTZ and (c) NI-N-PTZ. Decay trace of (b) NI-PTZ and (d) NI-N-PTZ at 420 nm. In deaerated ACN,  $c = 1 \times 10^{-4}$  M,  $\lambda_{ex} = 355$  nm, 20 °C.

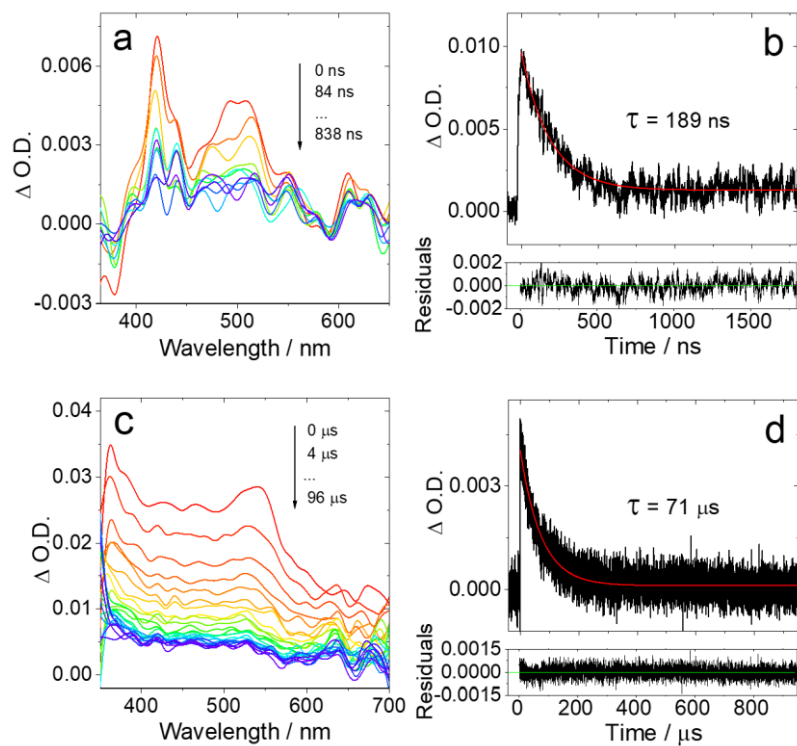


**Figure S35.** Nanosecond transient absorption of (a) NI-PTZ<sub>2</sub> ( $c = 1.0 \times 10^{-4}$  M) and (c) NI-PTZ-O ( $c = 1.0 \times 10^{-5}$  M). Decay traces of (b) NI-PTZ<sub>2</sub> ( $c = 1.0 \times 10^{-4}$  M) at 420 nm and (d) NI-PTZ-O ( $c = 1.0 \times 10^{-5}$  M) at 540 nm. In deaerated ACN,  $\lambda_{ex} = 355$  nm, 20 °C.

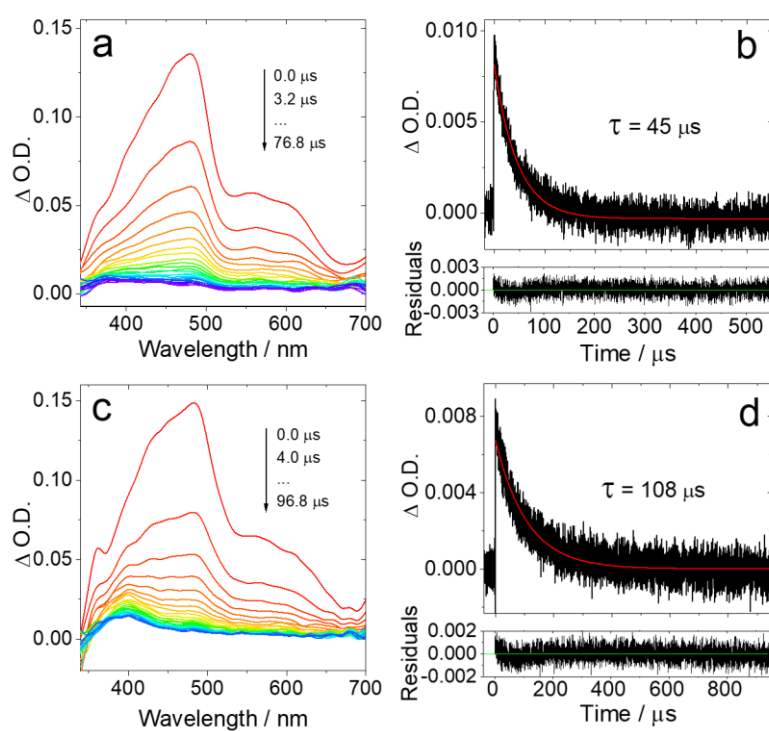


**Figure S36.** Nanosecond transient absorption of Ni-Ph-Br (a) in HEX and (c) in ACN,  $c = 5.0 \times 10^{-5}$

M. Decay traces of (b) in HEX and (d) in ACN,  $c = 2.0 \times 10^{-6}$  M,  $\lambda_{em} = 490$  nm,  $\lambda_{ex} = 355$  nm, 20 °C.

## 10. Calculated study

**Table S1.** Vertical absorption of **NI-N-PTZ**; **NI-PTZ**; **NI-PTZ-O**; **NI-PTZ<sub>2</sub>**; **NI-Ph-PTZ** and **NI-PhMe<sub>2</sub>-PTZ** (TDA-CAM-B3LYP/6-31G(d) in gas phase, in eV) along with their oscillator strengths (f) and major orbital contributions. The energy levels and major orbital contributions for T<sub>1</sub> and T<sub>2</sub> at the Franck-Condon region are also given.

Compounds	S <sub>1</sub> (absorption)				T <sub>1</sub>	T <sub>2</sub>
	$E_{\text{abs}}$ (eV)	f(a.u.)	C <sup>a</sup>	$\Delta E_{\text{vert}}$	C <sup>a</sup>	$\Delta E_{\text{vert}}$
	V)	/10 <sup>-4</sup>	MC <sup>b,c</sup>	(eV) <sup>d</sup>	MC <sup>b,c</sup>	eV) <sup>d</sup>
<b>NI-N-PTZ</b>	3.07	0	CT H-L (0.67)	2.69	LE H-2-L (0.65)	3.04 CT H-L (0.66)
<b>NI-PTZ</b>	3.17	1	CT H-L (0.67)	2.73	LE H-2-L (0.67)	3.12 CT H-L (0.64)
<b>NI-PTZ-O</b>	3.59	21	CT H-L (0.68)	2.74	LE H-2-L (0.67)	3.55 CT H-L (0.66)
<b>NI-PTZ<sub>2</sub></b>	3.06	1	CT H-L (0.67)	2.72	LE H-4-L (0.64)	3.00 CT H-L (0.65)
<b>NI-Ph-PTZ</b>	3.92	3	CT H-L (0.61)	2.67	LE H-2-L (0.61)	3.45 LE H-L+4 (0.36)
<b>NI-PhMe<sub>2</sub>-PTZ</b>	3.90	3	CT H-L (0.64)	2.71	LE H-2-L (0.66)	3.65 - H-4-L (0.56)

<sup>a</sup>Character; <sup>b</sup>Major contributions; <sup>c</sup>H and L represent HOMO and LUMO, respectively. Predominant HOMO→LUMO transitions for S<sub>1</sub>, T<sub>1</sub>, and T<sub>2</sub>, between brackets the corresponding coefficient; <sup>d</sup> $\Delta E_{\text{vert}}$  corresponds to the energy difference between GS and T<sub>1</sub> and T<sub>2</sub> at the FC region.

**Table S2.** Emission energies (TDA-CAM-B3LYP/6-31G(d) in gas phase, in eV) along with their oscillator strengths ( $f$ ) and major orbital contributions. The energy levels and major orbital contributions for  $S_1$ ,  $T_1$  and  $T_2$  are given at their respective optimal energy geometries.

Compounds	$S_1$ (emission)			$T_1$ (emission) <sup>e</sup>		$T_2$ (emission) <sup>e</sup>	
	$E_{\text{ems}}$	$C^a$	$f^d$	$E_{\text{ems}}$	$C^a$	$E_{\text{ems}}$	$C^a$
	/eV	MC <sup>b,c</sup>	/10 <sup>-4</sup>	/eV	MC <sup>b,c</sup>	eV	MC <sup>b,c</sup>
<b>NI-N-PTZ</b>	2.22	CT H-L (0.69)	0	1.93	LE/CT H-1-L (c: 0.5)/H-L (0.4)	-	-
<b>NI-PTZ</b>	2.21	CT H-L (0.69)	2	1.84	CT H-L (0.64)	2.01	LE H(-2)-L (0.68)
<b>NI-PTZ-O</b>	2.86	CT H-L (0.68)	1	2.02	LE H(-2)-L (0.68)	2.83	CT H-L (0.67)
<b>NI-PTZ<sub>2</sub></b>	2.09	CT H-L (0.69)	1	1.80	LE/CT H-1-L (0.63)	-	-
<b>NI-Ph-PTZ</b>	3.00	CT H-L (0.65)	0	2.01	LE H(-1)-L (0.66)	-	-
<b>NI-PhMe<sub>2</sub>-PTZ</b>	3.24	CT H-L (0.68)	447	2.02	LE H(-1)-L (0.60)	-	-

<sup>a</sup>Character; <sup>b</sup>Major contributions; <sup>c</sup>H and L represent HOMO and LUMO, respectively. Predominant HOMO→LUMO transitions for  $S_1$ ,  $T_1$ , and  $T_2$ , between brackets the corresponding coefficient;

<sup>d</sup>oscillator strengths, eV; <sup>e</sup> $f = 0$ .



**Table S3.** Calculated energy gaps at different regions of the photo deactivation decay (in eV) for **NI-PTZ** and **NI-PTZ-O**.

Molecule	$\Delta E_{S,T-GS}$ (eV) <sup>a</sup>			$\Delta E_{S-T}$ (eV)		$\Delta E_{T-GS}$ (S <sub>i</sub> , eV) <sup>b</sup>		$\Delta E_{S-T}$ (S <sub>i</sub> , eV)	
	<sup>1</sup> CT	<sup>3</sup> LE	<sup>3</sup> CT	<sup>1</sup> CT-	<sup>1</sup> CT-	<sup>3</sup> LE	<sup>3</sup> CT	<sup>1</sup> CT-	<sup>1</sup> CT-
<b>NI-PTZ</b>	2.60	2.37	2.14	0.23	0.46	2.74	2.57	-0.14	0.03
<b>NI-PTZ-O</b>	3.12	2.37	3.09	0.75	0.03	2.63	3.09	0.49	0.03

<sup>a</sup> $\Delta E_{S,T-GS}$  corresponds to the energy difference between the singlet (S) or triplet (T) minimum and the ground state (GS) minimum, i.e., adiabatic energy difference; <sup>b</sup>Relative energies at the S<sub>i</sub> optimized geometry, i.e., vertical energy difference.